Available online at www.sciencedirect.com
ScienceDirect
Journal of Molecular Graphics and Modelling 25 (2006) 126–145
Journal of Molecular Graphics and Modelling
www.elsevier.com/locate/JMGM

Molecular graphics approach to bacterial AcrB protein–β-lactam antibiotic molecular recognition in drug efflux mechanism☆

Rudolf Kiralj, Márcia M.C. Ferreira *

Laboratório de Quimiometria Teórica e Aplicada, Instituto de Química, Universidade Estadual de Campinas, Campinas, SP 13084-971, Brazil

Received 1 March 2005; received in revised form 30 August 2005; accepted 25 October 2005
Available online 6 January 2006

Abstract

AcrAB–TolC is the most important multidrug efflux pump system of Gram-negative bacteria, responsible for their resistance to lipophilic and amphiphilic drugs. In this work, a molecular graphics study of the pump components AcrB and TolC, 16 β-lactam antibiotics and 7 other substrates, as well as of AcrB–substrate complexes, was performed in order to give a mechanistic proposal for the efflux process at molecular level. AcrAB–TolC is a proton-dependent electromechanical device which opens to extrude drugs from the bacterial periplasm and perhaps cytoplasm, by means of a series of structural changes within the complex and its components AcrA, AcrB and TolC. These changes are initiated by protonation and disruption of salt bridges and certain hydrogen bonds, and are followed by conformational changes in which a number of intra- and interchain interactions are rearranged. Molecular properties of β-lactams accounting for their lipophilicity, shape/conformation and other sterical features, polar/charge group distribution and other electronic properties, and hydrogen bonding potency determine their interaction with polar headpieces of the inner membrane, recognition and binding to receptors of AcrB and TolC. The orientation of the β-lactam molecular dipoles with respect the efflux system is maintained during the drug efflux. Elongated cylinder-like β-lactam antibiotics with lipophylic side chains, a significantly negative component of the dipole moment and low hydrogen bonding capacity seem to be good substrates of AcrAB–TolC.

Keywords: AcrAB–TolC efflux pump; β-Lactam antibiotics; Multidrug resistance; Molecular graphics; Vestibules; Pore

1. Introduction

Transmembrane solute transporters serve the cell and its organelles in exchanging matter with the environment [1]. Over 150 families of transporters [2] exist in prokaryotes, archaea and eukaryotes [3,4]. Export transporters (efflux pumps) are known in human and animal cancer [3–7] and in microbes [3,4,8,9]. The pumps are one of the main mechanisms of multidrug resistance (MDR), turning resistant to a wide variety of structurally diverse compounds after prolonged anticancer or antimicrobial therapy [10–13]. Overuses and misuses of antimicrobials [9,12,14–17] also provoke MDR, resulting in mortality and therapy costs increase, infections in hospitals [12] and via food/industry products [14].

Drug design is one of the main strategies in combating MDR [12,15,16,18–20], directed towards inhibitors, modifiers/blockers of microbial [3,21,22] and cancer [6,11] pumps. However, the contribution of quantitative structure–activity relationship (QSAR) and molecular modeling publications is still modest. Those about cancer cells [23–26] (over 70 publications) deal mostly with P-glycoprotein, while those about bacteria [27–29] (some ten in total) are mainly concentrated on cytotoxicity aspects.

β-Lactam antibiotics act primarily as inhibitors of penicillin-binding proteins (PBPs) which build and maintain the bacterial cell wall. The β-lactam activity can be suppresed by MDR mechanisms such as the production of β-lactamases [30], changes in the outer cell membrane permeability, mutations of PBPs affinity for antibiotics [31], and the overproduction of MDR efflux pumps [8,32–37].

AcrAB–TolC efflux pump in *E. coli* [34,38], *S. typhimurium* [39], *S. enterica* [35], *H. influenza* [40] and other bacteria is intrinsically resistant to diverse lipophilic/amphiphilic toxic compounds from the bacterial natural environment and drugs

☆ A part of this paper was presented in the Eighth Scandinavian Symposium on Chemometrics, Mariehamn, Finland, 14–18 June 2003.

* Corresponding author. Tel.: +55 19 3788 3102; fax: +55 19 3788 3023.
E-mail address: marcia@iqm.unicamp.br (Márcia M.C. Ferreira).

1093-3263/$ – see front matter © 2005 Elsevier Inc. All rights reserved.
doi:10.1016/j.jmgm.2005.10.010

[8,32–34,41–43]. It is a channel-type secondary transporter [1,2] with proton influx (drug/H^+ antiport [8,44]). This pump is a tricomponent system [41] consisting of trimeric inner-membrane transporter AcrB [45–53] from the resistance-nodulation division superfamily of proteins (RND) [8], trimeric outer-membrane channel-tunnel protein TolC [45,54–60] from the TolC family [55,57], and periplasmic linker protein AcrA (probably trimeric) [58–60] from the membrane fusion family [61]. AcrAB–TolC exports xenobiotics from the cytoplasm/periplasm directly into the external medium [37,45,46,48–50,54] when all its components are coupled [38,41,59,62].

Structural studies of AcrA [58], AcrB [45–47,49–53] and TolC [54–56], and biochemical experiments [33,44,48,57,59,62–65] provide a new insight into structure–function relationship of AcrAB–TolC. Fig. 1A shows the pump external structure (electrostatic potential from WebLab ViewerPro 4.0 [66]) and its position in the cell. Fig. 1B and C show the trimeric structure and domains of AcrB. AcrB and TolC are from the Protein Data Bank [68,69] (1IWG [46] and 1EK9 [54], respectively). The lipophilic parts of TolC and AcrB lie in the membranes, similarly to cancer [67] and bacterial [9,71–75] efflux pumps.

The two proposed efflux mechanisms mediated by AcrAB–TolC [3,45,46,49–51,53–55,63,64] (Fig. 1) include substrate molecules located in the outer (periplasmic) and inner (cytoplasmic) leaflets of the inner membrane. The substrates access the AcrB central cavity through one of the three vestibules (openings) directly or passing through transmembrane grooves. The decrease of intracellular pH is the key of allosteric mechanism for opening of the AcrB and TolC channels [8,46,70].

According to the principles of pump–drug interactions [3,4], a good drug is a poor pump's substrate. In terms of minimal inhibitory concentration (MIC) [76], high MICs characterize good efflux substrates and effective efflux pumps. Channel-type pumps [1] possess a hydrophobic, amphiphilic or hydrophilic channel/pore through which substrates of similar characteristics are excreted. The channel system in AcrAB–TolC contains a few drug recognition/binding sites in AcrB

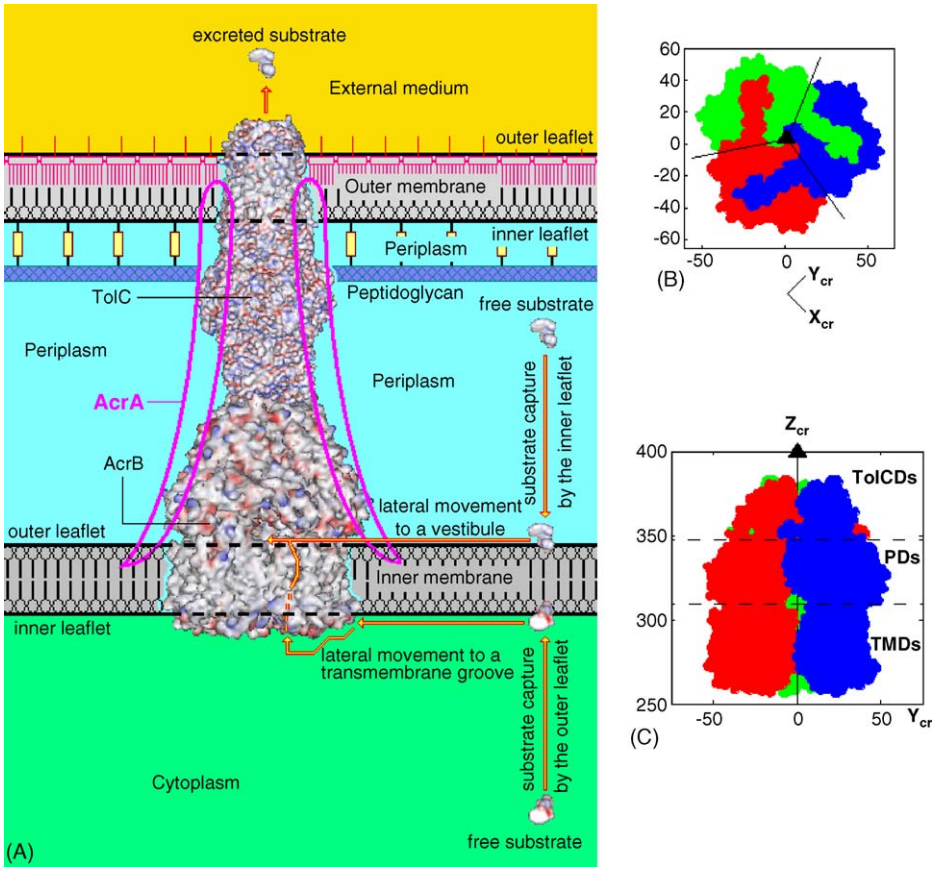

Fig. 1. (A) Combined 3D and schematic representation of the AcrAB–TolC efflux pump in an *E. coli* cell. The AcrB and TolC trimeric proteins are shown by electrostatic potential at molecular surface, based on crystal structures from Protein Data Bank (PDB: 1IWG and 1EK9, respectively) and generated hydrogen atoms. Hypothetical AcrA structure (two protomers are visible) is shown by pink sketch. Hydrophobic parts of AcrB and TolC placed in the inner and outer membrane, respectively, can be distinguished from hydrophilic by predominant color (gray for hydrophobic areas). Two main drug efflux mechanism are shown, one starting in the periplasm, and other in the cytoplasm. (B) and (C) Blue, red and green AcrB protomers around the three-fold crystallographic axis (Z_{cr} or C_3, ▲). Coordinates are in Å units. The position of the trimer with respect to Z_{cr} (crystallographic *c*) axis is visible. Axis X_{cr} is parallel to crystallographic *a*. Transmembrane domains (TMDs), periplasmic (PDs) and TolC domains (TolCDs) and their approximate borders (dashed lines paralell to $X_{cr}Y_{cr}$ plane) are shown. The vestibule plane is parallel to the TMDs–PDs bordering line. The vestibule positions are marked by the three lines meeting at the axis Z_{cr}, reflecting exact C_3 symmetry of AcrB protein. The vestibule formed by the blue and red protomers can be viewed along the axis X_{cr} as a hole after which comes the central cavity and the green protomer.

[45,46,50,51,53] and TolC [54,56]. The number of AcrAB–TolC copies in a cell depends on the overexpression of acrA, acrB and tolC genes [34,77] which may be induced by substrates [3]. The pump and its overexpression play the major role in MDR [34,39,43]. The substrate properties also influence MICs [27–29]. AcrB and RND pumps possess a large and flexible hydrophobic cavity for accomodation of diverse substrates [45,51,53,78,79]. The substrates of antibiotic efflux pumps [3,4,8,26,28,45,49,50] are structurally unrelated, amphiphilic or hydrophobic (frequently with aromatic/planar groups), with diverse ionic nature but preferably with ionizable groups. The substrates of cancer pumps have similar properties [10–12,45,67]. QSAR of compounds excreted by cancer [23–26] and bacteria [27–29] pumps include molecular features as lipophilicity, hydrogen bond capacity, molecular size/shape, polarizability and polar groups distribution.

In previous QSAR study [29] of 16 β-lactams (Fig. 2) excreted by the AcrAB–TolC pump in three strains of *S. typhimurium* [39], parsimonius PLS models included liphophilicity, electronic and hydrogen bonding descriptors. In the present work, the AcrAB–TolC mediated efflux mechanism of **1–16** is elucidated by means of molecular graphics and modeling of AcrAB–TolC and its substrates. Prediction of β-lactam position in AcrB was performed taking into account non-specific AcrB–drug interactions, relationships among molecular descriptors for **1–20**, and AcrB–drug (**17–20**) crystal structures [53]. Structurally diverse substrates **21–23** were used to generalize the obtained results.

2. Methods

2.1. Molecular modeling

Structures of **1–16** were from previous study [29], and of **17–20** from AcrB–drug complexes [53] (PDB: 1OYD, 1OYE, 1OY9 and 1OY8). Structures of **22** and **23** were from 3D Pharmaceutical Structure Database [80], and of **21** was modeled by PC Spartan Pro 1.0.5 [81] in extended conformation. The geometry of neutral or charged species (Fig. 2) was optimized at PM3 semi-empirical level, with fixed essential torsion angles in **17–20** to preserve bioactive conformation. Electronic and steric descriptors were calculated by Spartan package, and polarizability by PM3 in MOPAC 6.0 [82].

2.2. Molecular graphics

Molecular graphics was employed in qualitative and quantitative study of the AcrAB–TolC components (TolC: 1EJK9 [54], AcrB: 1IWG [46], 1OY6 [53]), substrates and the AcrB–substrate complexes using programs PLATON [83], WebLab ViewerPro [66], PC Spartan Pro and Matlab 5.2 [84]. Dimensions of substrates and proteins were determined from atomic coordinates with and without van der Waals radii, and from molecular printouts using empirical method of internal standards [85]. Topographic study of the AcrB trimer was performed from 4 Å depth slices along axes *X* and *Z*. Certain steric molecular descriptors were calculated directly from measured molecular dimensions and areas.

2.3. Prediction of β-lactams position and orientation inside the AcrB central cavity

Distance and angle parameters that define AcrB–drug (**17–20**) geometry in the crystal structures were measured from atomic coordinates and the position of drug inertial axes which were determined previously in calculations using MOPAC program. These parameters were then correlated with steric and electronic molecular descriptors via linear or non-linear regression. Due to observed systematic similarities between **17–20** and **1–16** with respect to selected descriptors, the regression equations were used to predict position and orientation parameters of β-lactams inside the AcrB central cavity.

2.4. Molecular mechanics of the pore tripeptid–drug complexes

Tripeptide complex formed by residues 96–112 from AcrB protomers (PDB: 1IWG) make the pore. A few selected drugs were modeled at the pore entrance and the complexes were treated by MMFF94 force field [86] in the Spartan program. The aim of this study was to detect the differentiation among the drugs with respect to their hydrogen binding capacity when interacting with the pore.

3. Results and discussion

3.1. Previous chemometric and QSAR results

Previous chemometric and QSAR analyses were carried out for 16 β-lactams (Fig. 2) [29]. The PCA–HCA (principal component and hierarchical cluster analysis [87–89]) study of in vitro pMICs (pMIC = −log MIC) related to a parent strain (SH5014), a mutant with overexpressed AcrAB–TolC (HN891), and a mutant with inactive pump (SH7616) of *S. typhimurium* [39], was carried out. β-Lactams were classified as good (**1**, **2**), moderately good (**3–9**, **14–16**) and poor (**10–13**) substrates. This agreed with experimental [3,4,50,67] and theoretical [28] findings that amphiphilic/lipophilic substrates had often planar aromatic substituents, lipophilic molecular ends and polar centers. In QSAR analysis, PLS (partial least squares [90,91]) models were constructed using lipophilicity, electronic and hydrogen bonding descriptors. Heteroatoms (also reported by Stanton et al. [28]), negative dipole moment *Y*-component D_y, and charged groups showed to be important for efflux activity. Charge transfer [92] and dipole moment and atomic charge changes occurs in β-lactams [93] in polar solvents. Polar headpieces of lipid bilayers, pump's charged/polar residues and exposed peptide bonds act as polar solvents to antibiotics. The PLS models [29] show that hydrophobic/polar groups (substrate domains [94]) of **1–16** interact with similar groups of the efflux system. Structures of AcrB and other RND pumps [45,51,53,78,79] show preference for these types of intermolecular interactions.

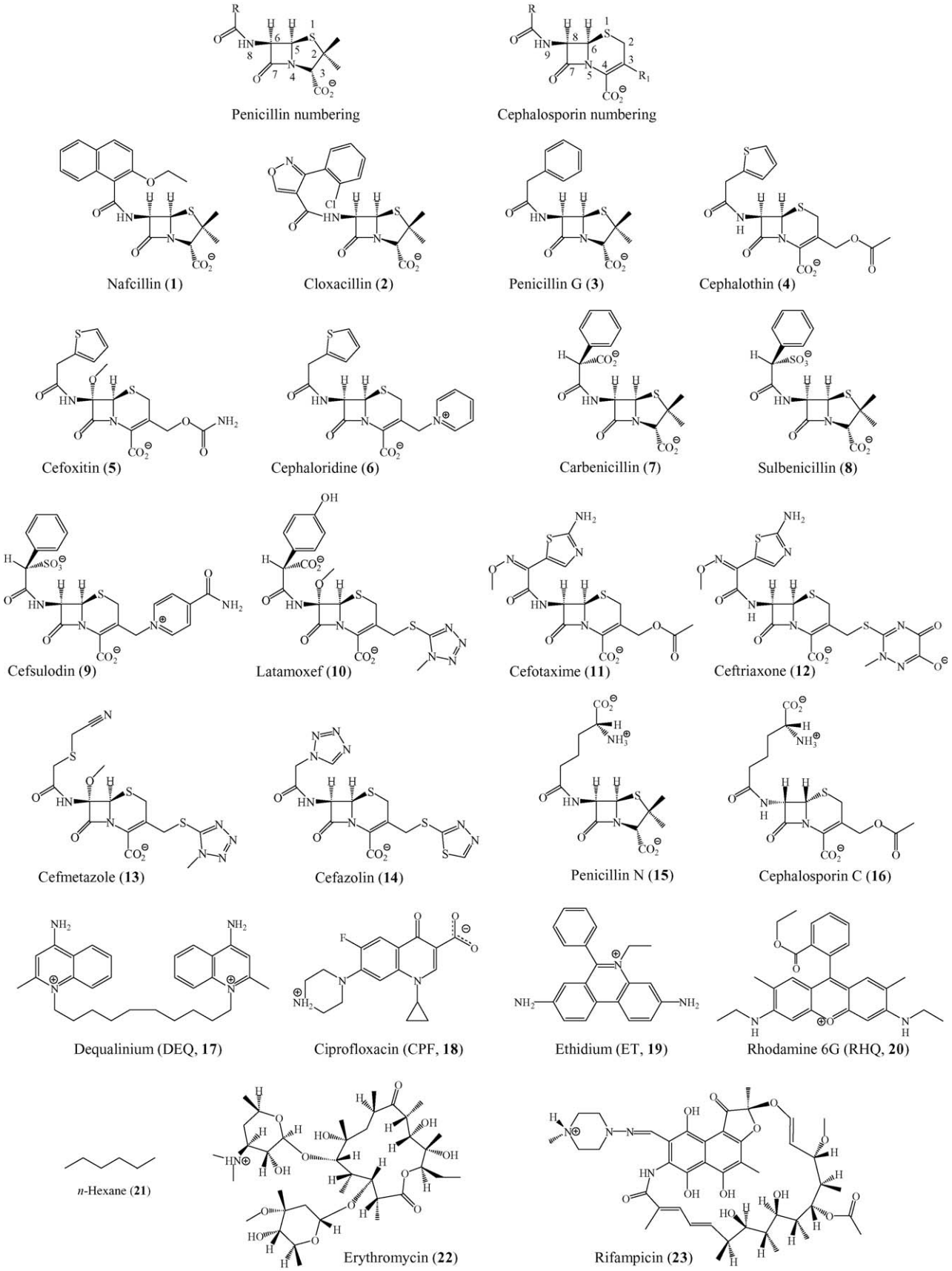

Fig. 2. Chemical structures of studied AcrAB–TolC substrates: β-lactam antibiotics (**1–16**) with atomic numbering and side chains for penicillins and cephalosporins, dequalinium (**17**), ciprofloxacin (**18**), ethidium (**19**), rhodamine 6G (**20**), *n*-hexane (**21**), erythromycin (**22**) and rifampicin (**23**).

3.2. Relationships between steric and electronic properties and activities for drugs *1–20*

Description of all molecular descriptors is in Table 1, and values for measured biological activities (pMICs) [34,35,39,71] and selected descriptors are in Table 2. Several pMIC–descriptor plots display **1–16** in at least two classes (Fig. 3: parallel curves or straight lines). Structurally diverse dequalinium (**17**, DEQ), ciprofloxacin (**18**, CPF), ethidium (**19**, ET) and rhodamine 6G (**20**, RHQ), with activity data properly scaled (Table 2), fit well among β-lactams. This means that β-lactam–pump interactions can generalized using AcrB–drug crystal structures [53]. Fig. 3 shows some representative pMIC–descriptor plots. Plots for strains HN891 and SH5014 are always very similar due to high correlation between the two activities [29]. The pMIC–molecular mass plot (Fig. 3a) shows that pMIC decreases with molecular size, what agrees with literature [24,25,28]. This is also visible in Fig. 3b, with the principal moment I_x: substrates with smaller I_x are easier exported from bacteria. The moments ratio I_{yx} (Fig. 3c) or I_{zx} (not shown) and other steric parameter confirm this finding when plotted versus pMIC: molecular area along axis *X*, i.e. projected on the principal plane *YZ* (S_x, Fig. 3d), *YZ* face area of the molecular box defined by atomic coordinates (A_{yz}, Fig. 3e), and *XY* face area (A_{xy} only for strain SH7616, Fig. 3f). The most rigid samples **1**, **2** and **9** with two five- or six-membered rings in R/R_1 form a group in several plots.

Several electronic properties also exhibit sample clustering and tendency to decrease linearly or non-linearly on pMICs: D_y (Fig. 3g), polarizability α (Fig. 3h), absolute *X*-component of

Table 1
List of molecular descriptors for drugs **1–20**

Symbol	Name and description	Nature[a]	Origin[b]	Ref.[c]
M_r	Relative molecular mass	steric	compos	tw
I_x	First principal moment of inertia (around axis *X*)	steric	comput	tw
I_y	Second principal moment of inertia (around axis *Y*)	steric	comput	tw
I_z	Third principal moment of inertia (around axis *Z*)	steric	comput	tw
I_{yx}	Ratio between the principal moments I_y/I_x	steric	comput	tw
I_{zx}	Ratio between the principal moments I_z/I_x	steric	comput	tw
I_{zy}	Ratio between the principal moments I_z/I_y	steric	comput	tw
S_x	Molecular area projected on the *YZ* plane (along *X* axis, in the CPK molecular model)	steric	molgrp	tw
$S_{\%}$	Ratio between the area S_x and the area of the *YZ* face of the molecular box defined by the farthest CPK spheres (in the CPK molecular model), expressed as %	steric	molgrp	tw
α	Molecular polarizability	electron	comput	tw
$\lvert\beta\rvert$	Absolute second-order molecular polarizability β	electron	comput	tw
$\lvert\beta_x\rvert$	Absolute *X* component of β	electron	comput	tw
γ	Third-order molecular polarizability	electron	comput	tw
D_x	*X* component of molecular dipole moment	electron	comput	pw, tw
D_y	*Y* component of molecular dipole moment	electron	comput	pw, tw
D_z	*Z* component of molecular dipole moment	electron	comput	pw, tw
n_x	Surface molecular density projected on the *YZ* plane, defined as N/S_x, where *N* is the number of atoms	steric	molgrp	tw
Δ_1	The length of the molecular box along the axis *X* (in the CPK molecular model)	steric	molgrp	tw
Δ_{12}	The width(*Y*)/height(*Z*) ratio of the *YZ* face of the molecular box (in the CPK molecular model)	steric	molgrp	tw
$W_{X\mathrm{m}}$	Maximum of (*X* coordinate $\pm$ *v* d*W* radius)	steric	comput	tw
$W_{Y\mathrm{D}}$	Difference between the maximum and minimum of (*Y* coordinate $\pm$ *v* d*W* radius)	steric	comput	tw
W_{zy}	Ratio between the $W_{Z\mathrm{D}}$ and $W_{Y\mathrm{D}}$ differences	steric	comput	tw
A_{xy}	Area of the *XY* face of the molecular box defined by the minimum and maximum atomic coordinates	steric	comput	tw
A_{yz}	Area of the *YZ* face of the molecular box defined by the minimum and maximum atomic coordinates	steric	comput	tw
A_{xyz}	Area of the molecular box defined by the minimum and maximum atomic coordinates	steric	comput	tw
Δ_{xy}	Ratio between the *X* and *Y* edges of the molecular box defined by the minimum and maximum atomic coordinates	steric	comput	tw
Δ_{xz}	Ratio between the *X* and *Z* edges of the molecular box defined by the minimum and maximum atomic coordinates	steric	comput	tw
Δ_{yz}	Ratio between the *Y* and *Z* edges of the molecular box defined by the minimum and maximum atomic coordinates	steric	comput	tw

[a] Nature of molecular descriptors: steric or electron = electronic.
[b] Origin or calculation method: compos = compositional, comput = computed and molgrp = molecular graphics descriptors.
[c] Reference: tw = this work, pw = previous work (for **1–16**) [29].

Table 2
Biological activities and selected molecular descriptors for prediction of AcrB–drug geometry

Drug	pMIC[a] (HN891)	pMIC[a] (SH5014)	pMIC[a] (SH7616)	$\|\beta\|$ (a.u.)	n_x (Å^{-2})	I_{zy}	W_{Xm} (Å)	W_{zy} (Å)	Δ_{xy}	Δ_{xz}
1	2.310	2.607	4.714	732.684	0.814(2)	1.132	7.64	0.752	1.425	2.198
2	2.629	2.930	5.338	675.756	0.657(2)	1.160	5.77	0.819	1.192	1.547
3	4.019	4.621	6.126	590.921	0.860(2)	1.128	7.96	0.833	1.986	2.448
4	4.695	4.996	5.598	524.055	0.650(2)	1.311	5.71	0.735	1.067	1.711
5	4.427	5.029	5.631	126.154	0.687(2)	1.388	5.57	0.737	0.984	1.664
6	4.715	4.715	5.017	868.306	0.729(2)	1.180	7.03	0.832	1.534	1.944
7	4.073	4.675	5.277	456.771	0.777(2)	1.034	7.13	0.918	1.735	1.965
8	4.112	4.714	5.316	382.357	0.728(3)	1.081	7.66	0.819	1.497	1.723
9	3.919	3.919	3.919	524.215	0.729(2)	1.223	6.49	0.860	1.134	1.382
10	6.318	6.637	6.637	180.111	0.721(2)	1.349	7.65	0.618	1.094	2.085
11	5.959	6.579	7.181	940.755	0.637(1)	1.062	6.54	1.018	1.610	1.549
12	6.364	6.665	6.966	1616.186	0.724(2)	1.046	8.82	0.872	1.756	2.193
13	5.674	5.975	5.975	526.968	0.740(2)	1.184	8.10	0.716	1.408	2.230
14	5.055	5.357	5.357	233.053	0.596(1)	1.497	7.23	0.657	0.968	1.901
15	4.652	4.652	4.652	106.688	0.787(2)	1.260	6.86	0.856	1.361	1.701
16	4.414	4.414	4.414	54.813	0.961(3)	1.253	8.10	0.725	2.017	2.784
17	2.552[b]	2.853[b]	5.262[c]	218.619	1.159(3)	1.169	9.57	0.720	1.955	4.040
18	6.742[d]	7.043[d]	8.122[c]	1349.693	0.992(3)	1.246	8.07	0.606	1.492	3.075
19	2.293[e]	2.594[e]	5.003[c]	1194.951	0.973(3)	1.512	6.77	0.581	1.267	2.679
20	2.540[b]	2.841[b]	5.249[c]	2598.647	0.800(2)	1.380	9.09	0.853	1.498	1.828

[a] Efflux activity defined as pMIC = −log MIC, where MIC is molar concentration. Data from Nikaido et al. [39] for β-lactams **1**–**16**.
[b] Adopted values MIC(HN891) = 1280 and MIC(SH5014) = 640 μg/ml for DEQ and RHQ, assuming identical behavior of these drugs with respect to ET. Based on data from Sulavik et al. [34] and Tikhonova et al. [71].
[c] Data for an AcrAB gene deleted strain from *E. coli* published by Sulavik et al. [34].
[d] Data for strains HN891 and SH5014 from Giraud et al. [35].
[e] Value MIC = 800 640 μg/ml from Tikhonova et al. [71] for a wild AcrAB strain of *E. coli* was used for strain SH5014, and doubled value for HN891.

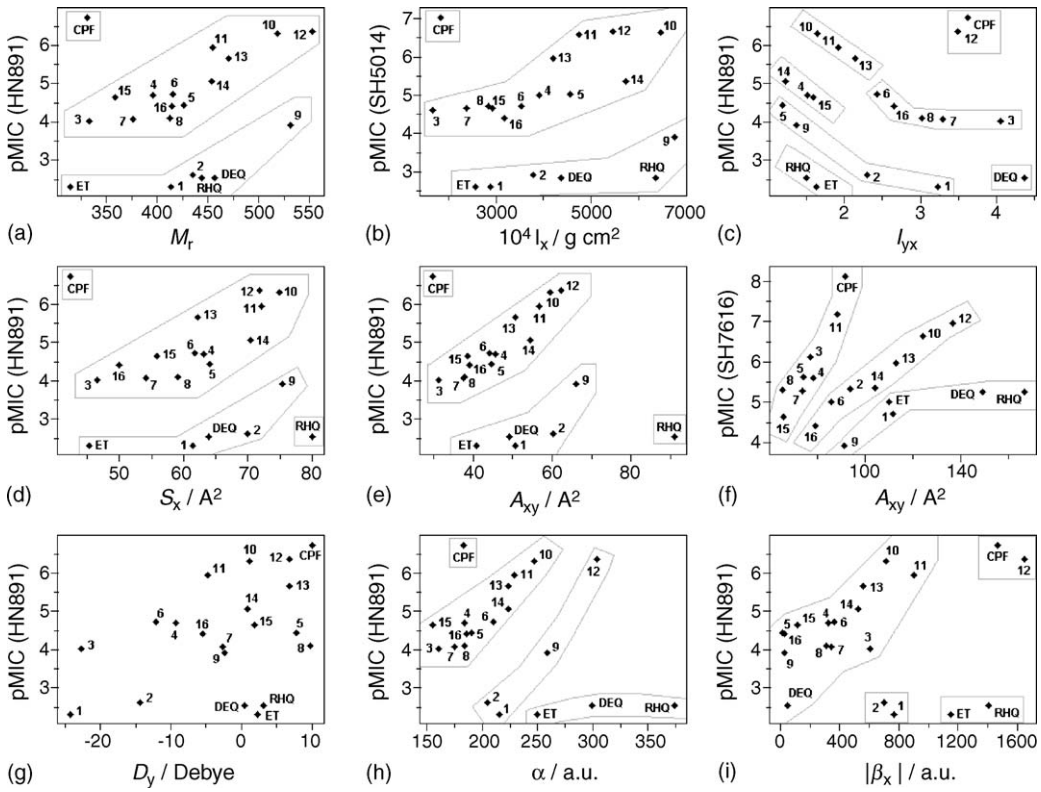

Fig. 3. Some representative efflux activity–drug molecular descriptor plots important for elucidation of the efflux mechanism: (a) pMIC(HN891), M_r; (b) pMIC(SH5014), I_x; (c) pMIC(HN891), I_{yx}; (d) pMIC(HN891), S_x; (e) pMIC(SH5014), A_{yz}; (f) pMIC(SH7616), A_{xy}; (g) pMIC(HN891), D_y; (h) pMIC(HN891), α; (i) pMIC(HN891), $|\beta_x|$. See Table 1 for definition of molecular descriptors.

the second-order polarizability β ($|\beta_x|$, Fig. 3i), and the third-order polarizability γ (not shown). Consequently, hydrophobic groups are less polarizable than hydrophilic, and lipophilic molecules are better substrates.

High correlations among the principal moments (I_y–I_z: 0.970, I_{yx}–I_{zx}: 0.977) and other steric relationships indicate an overall cylinder-like shaped **1**–**20** along *X* axis, with circular to eliptical projection on the *YZ* plane (Figs. 4 and 5). Elongated cylinders are ideal forms to pass through channels and grooves (see Fig. 4). The bullet shape of β-lactams facilitates their porin-mediated influx [17]. In general, molecular shape, branching and conformation influence efflux activity [23,28]. Stanton et al. [28], using conformation-dependent descriptors (length/thickness and length/breadth ratio), concluded that heteroatoms made substrates more branched, less linear, hydrophobic and rigid, what can be said also about **1**–**20**.

D_y was included into two PLS models. D_y vector in the best substrates (**1**, **2**) is placed between the β-lactam ring and side-chain R, meaning that the ring is predominantly negative (hydrophilic) and R is positive (hydrophobic). Fig. 5 shows that D_x has a role in the efflux of **1**–**20**, while the importance of D_z is minor. Substrates **21**–**23** have quite different behavior. The axes *X* and *Y* might be directions of drug motion through the efflux system due to spatial consistency between steric and electronic properties.

3.3. Molecular graphics of the AcrAB–TolC external and internal structure

AcrAB–TolC is the major contributor to intrinsic MDR in *E. coli* [34], and the most effective RND pump [94]. Its homologs have high sequence identity [95], similar structure and efflux mechanism.

3.3.1. AcrA

AcrA (Fig. 1A) is an auxiliary transport protein [1] with lipophylic transmembrane segment (TMS) close to the N-terminus [2]. This end might be located in the inner membrane like in its homolog MexA [74], while the C-terminus interacts with AcrB [96]. 3D structure of functional AcrA is still unknown [94]. AcrA protomer is probably a helix [58], not a coiled-coil [55]. Although MexAB-OprM pump [72] is highly homologous to AcrAB–TolC [71,73,97], the structure of functional MexA [74,75] cannot be applied to AcrA. Murakami and Yamaguchi [45] consider both elongated and coiled-coil forms in pump resting and functional state, respectively. AcrA binds both to AcrB and TolC [45,46] and maybe to the membranes. Proton influx induces reversible oligomerization (via S–S bonds) and conformational changes of AcrA [60], bringing it into strong interactions with TolC and AcrB. These changes propagate into TolC and AcrB, up to opening the efflux pathway [45,55,60].

3.3.2. TolC

It is a channel-tunnel periplasmic protein (Fig. 1A) that excretes a wide range of macromolecules, small molecules and heavy metals [55,56] as the outer membrane component of several efflux pumps [94]. A TolC protomer has three TMSs forming a porin-like β-barrel domain placed in the outer membrane (Fig. 1A). The long and wide cylinder (tunnel domain) [54–56] consists mainly of α-helices and connects the outer membrane with the AcrB during the efflux process. Its thick part is a mixed α/β equatorial domain [56,94] that interacts directly with AcrA by docking the TolC bottom into the cone-like AcrB funnel [55,62]. TolC ends at the outer leaflet of the outer membrane as three coiled-coils (Fig. 4B), similarly to the TolC pore at the TolC bottom [55,94,98]. The pore (six Asp residues) is 3–4 Å in diameter when closed, and 20–25 Å

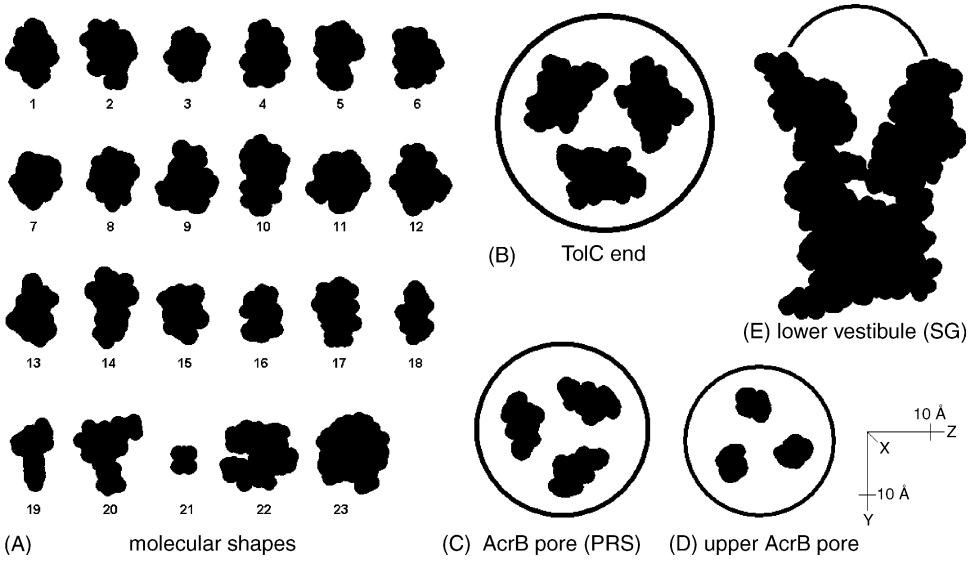

Fig. 4. (A) Molecular shapes of **1**–**23** as viewed along the principal axis *X* with orientation of the principal axes *Y* and *Z* with scale (right down). The shapes of important channels and grooves of AcrAB–TolC: (B) the coiled coils (Ala269-Tyr274) of the TolC end (PDB: 1EK9); (C) the PRS (Asp99, Asp101) at the pore entrance; (D) the upper part of the pore channel (Gln112) representing the overall internal pore dimensions (PDB: 1IWG); (E) the south groove (SG) of the vestibule BRAMLA area (PDB: 1IWG) formed by the left and right helices (Asp7-Val32 and Gly870-Glu896, respectively). All representation were done by using PLATON program.

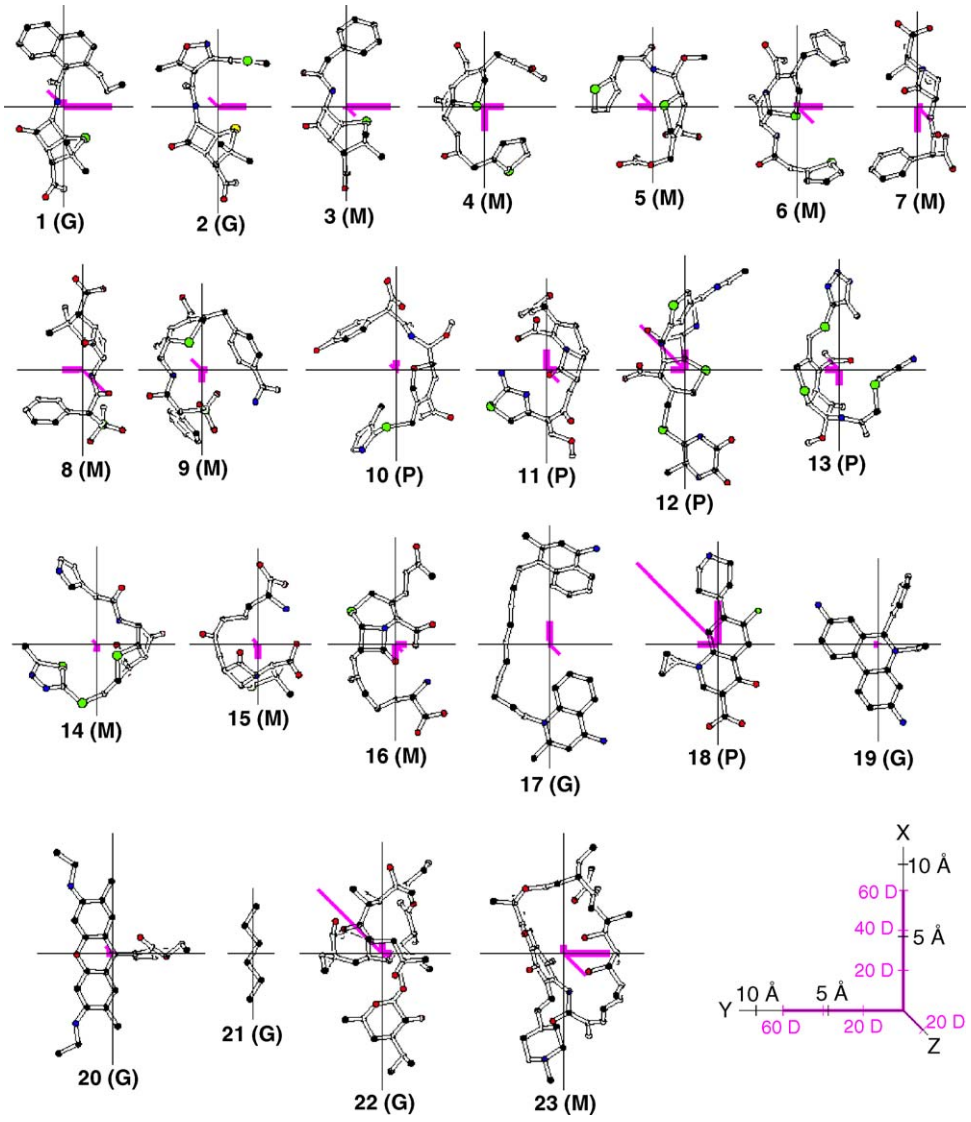

Fig. 5. Molecules **1**–**23** with principal axes, dipole moment components and corresponding scales (Å - ångstrom and D -Debye units). Plane *XY* is the plane of projection. Hydrogen atoms are omitted because of clarity. Molecules are marked as good (G), moderately good (G) and poor (P) substrates of the AcrAB–TolC efflux pump.

when open [55,94]. Its coiled-coils are interconnected by salt bridges and hydrogen bonds that disrupt by protonation and AcrA-induced conformational changes [56]. The TolC pore can be blocked by larger polyvalent metals [98], drugs with several charged groups as polycations, and probably with the β-lactams characterized previously [29] as poor substrates.

3.3.3. AcrB

AcrB is a protein efflux pump from the RND superfamily [8,32]. An AcrB protomer has twelve lipophylic TMSs [2,32,99], two large periplasmic loops, and four conserved motifs [8,9,52] (one in the periplasmic loop, three in the segments). Three protomers form the functional jellyfish pump [45,46,49] (Fig. 1A and C). As AcrB crystallizes in trigonal space groups [45–47,49], its three-fold molecular (Z_{cr}) and crystallographic (c) axes coincide, and the axis passing through a vestibule (X_{cr}) is parallel to a crystallographic axis perpendicular to c (Fig. 1B and C). The protomers are tightly bound (Fig. 1 right top) forming the complex (130 Å × 120 Å; Fig. 1C, 1IWG). The bottom, transmembrane region, consists of 36 TMSs (three transmembrane domains, TMDs), and their bottom connections already lie in cytoplasm. The upper region, the periplasmic headpiece, is formed by six periplasmic loops which are responsible for substrate specificity [65]. It consists of three pore domains (PDs) positioned around the pore, and three TolC domains (TolCDs) that can connect to the TolC bottom. TMDs (50 Å height [46]) are in the inner membrane. The plane between the PDs and TMDs (midway between Pro31 and Asp301) is the vestibule plane (VP). Its intersection with the line of interaction of protomers defines the position of a vestibule (Fig. 1B and C). The periplasmic headpiece and transmembrane region can be seen in Fig. 6B and D relative to the VP. Each protomer has two Asp-Lys ions pairs in TMD. Proton influx disrupts these bonds via Asp protonation and

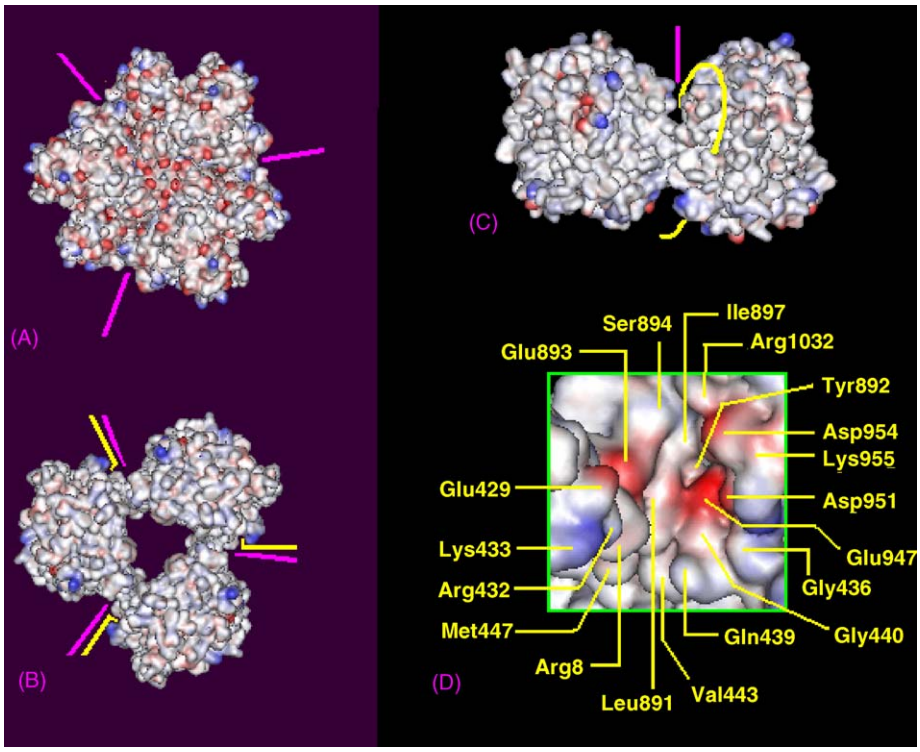

Fig. 6. Electrostatic potential representation (red: negative; blue: positive; white: zero): (A) of the pore domains (PDs), and (B) the transmembrane domains (TMDs) viewed upwards and downwards the vestibules plane, respectively. (C) The transmembrane groove (TMG) circular shape and position at the TMDs surface. The position of the vestibules (pink line) and the TMGs (yellow circle). (D) The TMG pore at its entrance, with its residues. Structure from the Protein Data Bank (PDB: 1IWG).

causes conformational changes within the AcrB trimer and the AcrB pore opening [45,46,49]. The proton and the substrate translocation pathways may be separated by at least 6 Å [44].

3.3.4. Vestibules

These three openings, through which substrates from periplasm enter the central cavity [45,46,49–51,53,63], are formed by pairs of AcrB protomers (Figs. 1 and 6). A vestibule consists of the entrance, channel and end (Fig. 7A) which possess several neutral and charged residues involved in attraction/selection of substrates from the periplasm [51]. The channel size and shape vary in space. Viewing from the VP upwards (topographic analysis, Fig. 7A), the channel is wide at the entrance (13 Å, 1IWG) and shallow in the PDs. Viewing from VP downwards, it is narrow and deep in the TMDs. Its overall length is 11 Å. In another topographic analysis

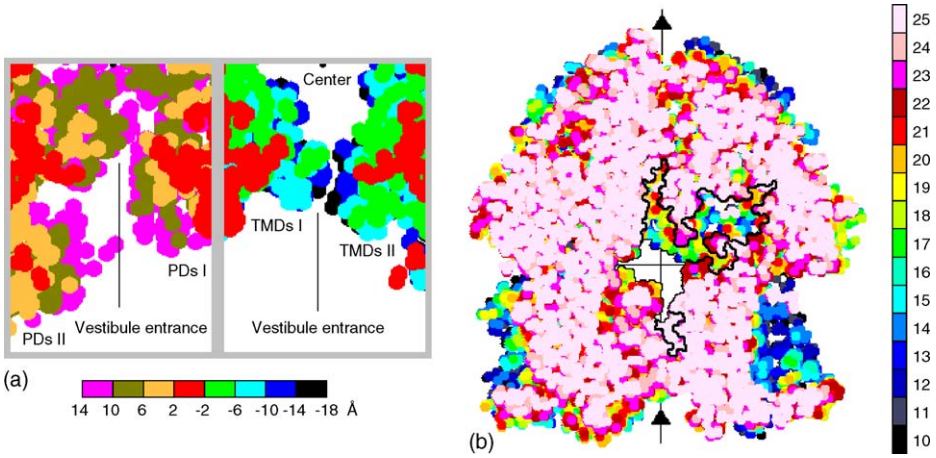

Fig. 7. (a) Topographic map of a vestibule and its surroundings viewed upwards (left) and downwards (right) the C_3 symmetry axis. The heights of the layers are given with respect the vestibule plane. Protomers I and II are the former blue and red (as in Fig. 1B), respectively. (b) Topographic map of AcrB transport protein presented by 16 slices. The heights are the slice distances from the trimer axis (in Å). Two pockets in the PDs region (the slice at 22 Å), and the inner cleft at the end of the vestibule (the slice at 19 Å), are drawn as solid curved lines. Structure from the Protein Data Bank (PDB: 1IWG).

(Fig. 6B), the superposition of 16 slides at 10–25 Å from Z_{cr} displays the vestibule shape. The vestibule below VP is formed by two hydrophobic α-helical TMSs (see Fig. 4E), and above VP is made by several coils and two short α-helices from the PDs. Two big inner pockets per protomer (best visible at 22 Å from Z_{cr}) and an inner cleft are connected to a vestibule. Fig. 8 depicts the vestibule features along X_{cr}. The lower and upper entrances were shaped mostly by hydrophobic and polar residues, respectively (Fig. 8a). Hydrogen bond donors and acceptors as well as charged residues are distributed in a similar way (Fig. 8b). Electrostatic potential (Fig. 8c) confirms that the vestibule hydrophobic character decreases from the bottom to the top, from left to right, and from the entrance to the end. For qualitative consideration of vestibules, a useful concept of BRAMLA (BRAzil Map-Like Area, reminding on the map of Brazil) was introduced (Fig. 8d and e). It is the area visible in vestibule projection as in Fig. 8a–c, the minimum free area shaped by the vestibule and central cavity. The green BRAMLA fraction can be superimposed to a substrate image without overlapping any residue. Two-third of BRAMLA lies in hydrophobic region. BRAMLA dimensions are in Fig. 8d (1IWG). BRAMLA is surrounded by W and E ceiling, small W, SW and great W wall, and small CW plateau, as well as SG (south groove) bottom. The main channel can be divided into W and E parts. Deep SG (Fig. 4E) is surrounded by hydrophobic residues in its lower part (lower SG, LSG), and by hydrophilic in its upper part (upper SG, USG). Narrow LSG (1.6 Å) corresponds to a channel (3.5–3.9 Å) through which a hydrophobic linear chain (**21**) or a planar fragment (**19**) may pass (Fig. 4E). Drugs **17**–**20** must have entered the central cavity bypassing through SG (Fig. 9). All of them are placed after SG and E main channel. LSG and USG are at the same height as hydrophobic chains and polar headpieces of the lipid bilayer, respectively. This is supported by that the vertical distance between CW plateau top and the AcrB bottom is 35 Å, being practically equal to the average vertical length of the TMSs (as defined by Fujihira et al. [99]) and to the thickness of lipid bilayer (30 Å) [100–102]. The depth of SG is 12.4–13.5 Å in the all AcrB-containing crystal structures, and that of the USG is 7.1–7.8 Å (size of a polar headpiece).

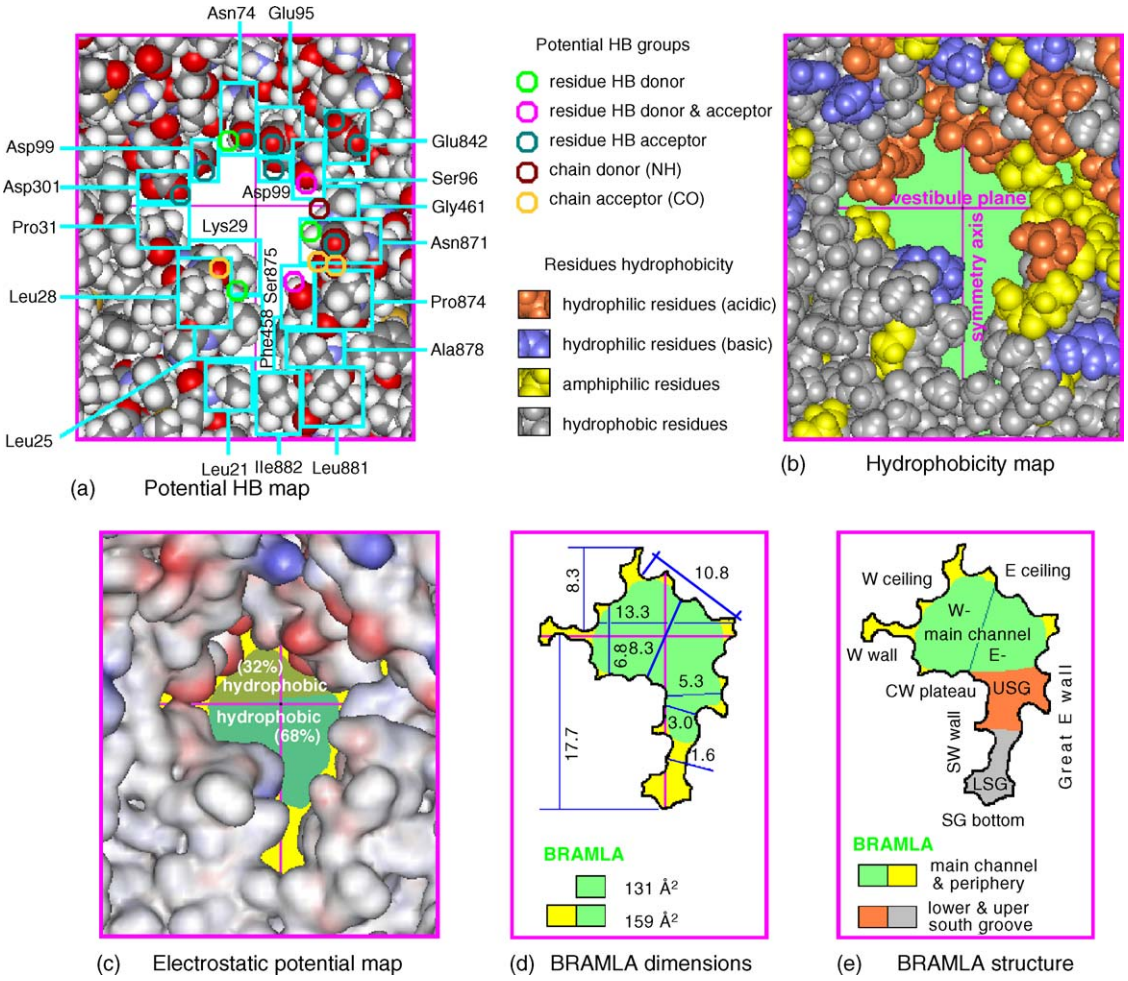

Fig. 8. The ID card of a vestibule and its 2D representation BRAMLA. (a) Potential hydrogen bonding groups from amino-acid residues and polypeptide chains are marked at the vestibule entrance and in the channel (CPK model). (b) The hydrophobic character of the essential residues is showed in the next figure (CPK model). (c) The electrostatic potential map (red: positive, blue: negative, white: neutral) shows the predominant hydrophilic and hydrophobic character of the upper and lower part of the vestubule with respect to the vestibule plane. (d) and (e) BRAMLA area is characterized by its dimensions (d) and distinct regions of both its interior and exterior (e). W, E, CW and SW abbreviations have geographical meaning: west, east, central west and south-west, respectively.

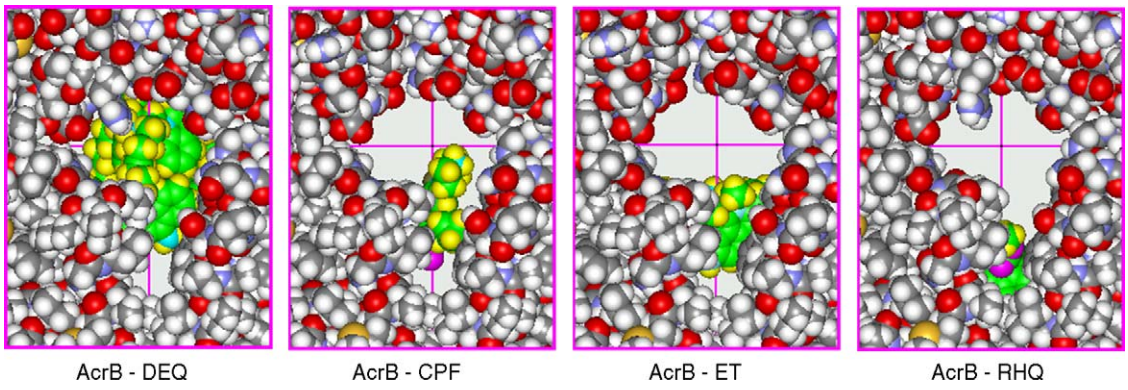

Fig. 9. CPK representation of a vestibule from crystal structures of the AcrB protein complexed by substrates DEQ, CPF, ET and RHQ (PDB: 1OYD, 1OYE, 1OY9 and 1OY8, respectively). The substrates are colored differently from the vestibule.

3.3.5. Transmembrane grooves (TMGs)

They translocate substrates from the cytoplasm to vestibules [45,46,49,50]. A TMG is almost parallel to SG (Fig. 6C), consisting of three TMSs of a protomer. There is a small hydrophilic pocket at cytoplasmic side (Fig. 6D), made by a TMS and a conserved motif. TMG extends on the TMD exterior, right to the great E wall (the bay right to the lower vestibule, Fig. 7A). The lipid bilayer closes the TMG into a channel. A substrate from cytoplasm, after leaving TMG, passes above the E wall and falls into SG, using the space of the right big inner pocket (Fig. 7B). Two RND motifs are probably involved in proton translocation when two bridges Lys-Asp disrupt [49].

3.3.6. The central cavity

This hole around the trimer axis (Z_{cr} or C_3 in crystal) is filled in its lower part by phospholipid bilayer [46,51,53]. Its upper part (30–35 Å × 15 Å) [45,46,49,51,53] is connected to the vestibules and big inner pockets. It has trigonal shape (Fig. 6C) and cross-section area 1400 Å^2 for 21 phospholipids (a headpiece covers 65 Å^2 [48]). AcrB–drug complexes [51,53] (Fig. 9) vary in drug position/orientation with respect to X_{cr}, Y_{cr}, Z_{cr}, residues and polar headpieces [53], sometimes with self-association (DEQ, ET [51,53]). The upper central cavity (<5000 Å^3) collects several molecules [53] which induce a small (1°) rotation of AcrB [53] and local changes (W ceiling of BRAMLA in Fig. 9).

3.3.7. The pore

This narrow channel connects the central cavity and funnel. Substrates are excreted through the pore after proton influx-induced changes [45,46,49,51,54]. The pore axis and Z_{cr} coincide, placing the pore in the middle of PDs (Fig. 6A). It is formed by three helices (21 residues, Asp 99-Pro 119, 45 × 10 Å; Fig. 10A and B). Three parts are well visible (Fig. 10C–E): the opening (pore recognition site, PRS), middle and the upper part. PRS is a cone-like pocket 8 Å deep, formed by highly hydrophilic (Asp99 and Asp101 triads) and liphophilic residues (Ile102, Ala103, Gln104, Val105, Fig. 10F). The middle is completely closed by Val105 and Asn109. The pore is amphiphilic in average (Fig. 10C). Several hydrogen bond donor and acceptor groups in residues and peptide bonds can interact with a substrate (Fig. 10F). Murakami et al. [52] reported five essential residues (Asp101, Asp109, Val105, Gln112, Pro116) oriented towards the pore interior. Ile102 can be also considered as essential, i.e. can interact with a substrate. There are two pore opening models: the pore middle part opens uniformly and the other parts extend [51,52,54]; or the pore middle part opens by substrate-induced local conformation changes, while the other parts open as in previous case [45]. In the latter mechanism, the middle part opens only partially during its interaction with a substrate molecule, and closes immediately after the substrate has passed. A drug is actively transported through the pore if the pore binding affinity for the drug decreases along the drug translocation direction [45]. When the pore middle part is closed, the PRS and the upper part can accommodate only small chain- (**21**) or planar-like molecules (**18**, **19**) (Fig. 4C and D). The pore tightest part is stabilized by nine putative hydrogen bonds established in the triad of Asn109 and of Gln112. These residues act both as hydrogen donors and acceptors, and thus have important functions as in proteins and protein-containing complexes [103]. The geometry of the Gln and Asp trimers was optimized by CHEM3D [104] at MM2 [105] level, and inserted into the structure in Fig. 10G and H. The pore helices must become more distant from each other to disrupt these bonds. Each helix is a part of the conserved motif *D* in RND pumps [8,9,52] (Fig. 10G). When the hydrogen bonds (Fig. 10H) are broken, the helices move around Z_{cr} axis and get straighter. These elastic movements are compensated in the motifs *D* which act like a triple spring by moving into the large inner pockets (Fig. 7B). The pore is now in open state, but its middle channel is still narrow. Then, a substrate molecule interacts with the PRS and the pore extends sufficiently for the substrate to pass, and contracts as the substrate has gone. The pore must open quite extensively [51] because of six essential residues and Asp99 that are turned against or perpendicularly to the substrate translocation direction: the angles between this direction and C_α–C_β bonds are 42–90° (1OY6). Such orientation of Asn109 and Gln112 facilitates the disruption of their hydrogen bonds (Fig. 10H). As conformational changes in the pore increase the distance between the hydrogen bond

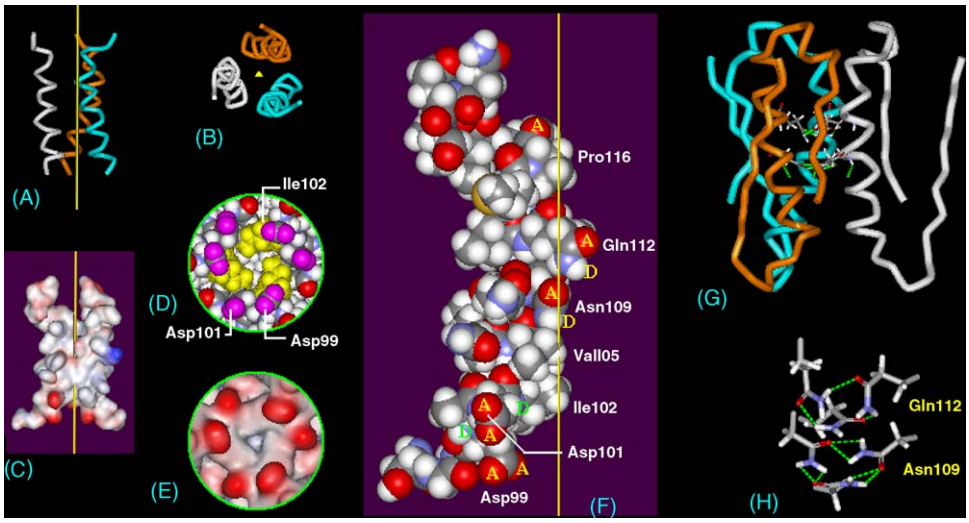

Fig. 10. The structure of the AcrB pore channel viewed perpendicularly to (A) and along with (B) the trimer C_3 axis. (C) The electrostatic potential representation of the pore channel interior excluding one pore helix. The structure of the pore recognition site represented by CPK model (D) and electrostatic potential surface (E). Quasi-hexagonal arrangement of charged Asp99 and Asp101 carboxylates (pink) and trigonal symmetry of hydrophobic Ile102 residues (yellow) in the PRS pocket is visible. (F) A pore helix from a protomer represented by CPK model and marked hydrogen bond donor (D in picture) and acceptor (A in picture) groups from amino-acid residues (yellow) and the polypeptide chain (green). (G) Three RND conserved motifs A including the pore with hdyrogen bonding residues that keep the pore tight. (H) These residues with their hydrogen bond network. Structures from the Protein Data Bank (PDB: 1IWG, 1OY6).

donors/acceptors, the closest donors/acceptors situated right below these residues tend to establish new hydrogen bonds which would turn away the Asn and Gln residues. Hydrophilic β-lactams can interact with the PRS or essential residues via hydrogen bonds or electrostatic interactions, what makes such compounds to be bad substrates.

3.4. Relationships between substrate molecular structure and its position in the AcrB central cavity

The most stable conformers for **1**–**16** obtained in previous QSAR study [29] were used in this work. Bioactive conformers for **18**–**20** (from AcrB–drug crystal structures) were preserved in all modeling studies. The extended (*trans*, *trans*, *trans*) conformer of flexible **21** was used as the most suitable to pass narrow channels. Drugs **22** and **23**, due to their macrocyclic structure, internal hydrogen bonds and elecrostatic interactions, are rather rigid. Hence, their retrieved structures [80] were used.

Trimeric AcrB is complexed by three drug molecules (**17**–**20**) related by C_3 axis inside the central cavity via hydrophobic, π···π stacking, electrostatic, van der Waals, hydrogen bond and other weak interactions [53]. The absence of close cation–anion interactions at the ceiling or pore has been commented by Yu et al. [53] as a consequence of hydrophobic/hydrophilic drug–protein and drug–polar headpieces interactions. Quantum-chemical modeling of **17**–**20** shows that all charges of the formally charged groups (Fig. 2), except that of NH_2^+ in CPF, are highly delocalized. Such diffuse charges cannot interact with particular anionic residues. Cationic drugs cannot be partitioned in a lipid bilayer unlike anionic/amphiphilic species due to high positive potential of the bilayer [51], meaning that **17**–**20** should be positioned closer to the pore, reaching the level of the CW plateau.

Distances and angle ε of AcrB–drug geometry are defined in Fig. 11, and experimental values are in Table 3. These values were used to predict the position and orientation of β-lactams in the AcrB central cavity, based on structural analogy between **1**–

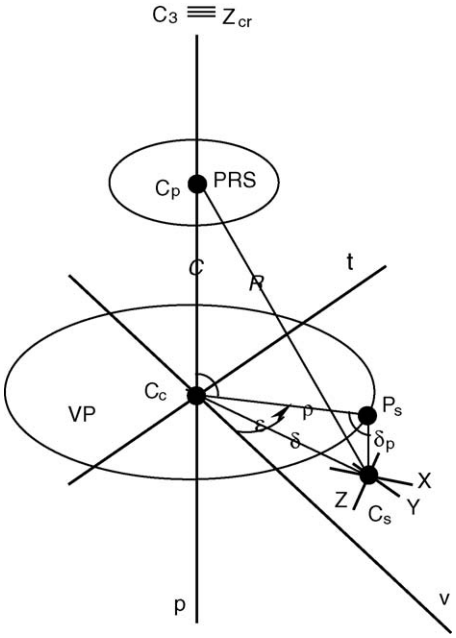

Fig. 11. Definition of parameters describing the AcrB–substrate geometry. The AcrB coordinate system is defined by the C_3 axis (p) parallel to the $-Z_{rc}$, the vestibule axis (v) parallel to the X_{cr}, and the third axis (t) parallel to the Y_{cr}. The axes v and t define the vestibule plane. The origin of the coordinate system is at the central cavity center (C_c), while the pore recognition site center (C_s) is situated at the axis p. The substrate center of mass (C_s) is projected on the vestibule plane (P_s). X, Y, Z are the substrate principal axes. Distance parameters d are defined as follows: $C = d(C_c, C_p)$, $R = d(C_p, C_s)$, $\rho = d(C_c, P_s)$, $\delta = d(C_c, C_s)$, $\delta_p = d(P_s, C_s)$. The angle ε is the substrate angular deviation from the vestibule axis.

Table 3
Experimental AcrB–substrate geometry

Parameter	DEQ (**17**)	CPF (**18**)	ET (**19**)	RHQ (**20**)
C (Å)	7.24	6.29	6.34	7.30
δ_p (Å)	2.64	7.20	8.28	15.02
δ (Å)	5.20	14.94	9.72	17.29
ρ (Å)	4.48	13.09	5.09	8.55
R (Å)	10.85	18.80	15.48	23.91
A_{xv} (°)	88.3	73.0	98.8	87.2
A_{yv} (°)	70.3	149.7	73.1	99.3
A_{zv} (°)	160.2	65.7	19.3	9.8
A_{xp} (°)	151.0	158.6	82.5	97.9
A_{yp} (°)	116.5	110.8	19.7	168.2
A_{zp} (°)	100.9	94.9	71.5	98.9
ε (°)	78.3	4.0	−11.4	−1.4
Π_{xpv} (°)	15.1	77.4	168.4	171.7
Π_{ypv} (°)	116.5	111.0	80.2	82.8
Π_{zpv} (°)	100.9	155.2	95.3	85.9
Π_{xypv} (°)	100.9	21.3	96.1	86.0

16 and **17**–**20**. As there are only four available complexes for data analysis, univariate linear/log-linear and parabolic relationships between the drug molecular descriptors (Tables 1 and 2) and geometry parameters (Table 3) were established (Table 4) under following conditions. (1) One to three descriptors of distinct nature/origin, and having high correlation with dependent variables (0.822–0.999) were selected, and the predicted values were averaged. (2) Uniform distribution of the four points along line or curve in the scatterplots to avoid chance correlation, was assumed. (3) Descriptors without extrapolated predictions, and with reasonable chemical interpretation of the results, were selected (Table 4). (4) Reasonable statistics (regression coefficient errors, Student test probability, experimental-calculated correlation and deviation) for the selected equations was assumed. The distance R from the ligand center to the PRS center (the center of Asp carbonyl oxygens closest to VP) and the distance to C_c (intersection of VB and Z_{cr}) significantly vary for **17**–**20**. CPF is closest to the vestibule end (largest ρ, see Fig. 11), while RHQ is at the lowest position with respect to VP. Angle ε defines the orientation of a drug relative to the vestibule axis (X_{cr} or v), and shows variation of almost 90°. Angles A and Π define the orientation of the positive end of the substrate principal axes (X, Y, Z) with respect to the positive ends of the p (negative Z_{cr}) and v (X_{cr}) axes (Fig. 11). These parameters show that the XY plane of DEQ, ET and RHQ is nearly coplanar to pv, and that of CPF is slightly tilted (by 21°). Predicted distances and angles for β-lactams are in Table 4, based on descriptors given in Table 2. The maximum errors center of mass coordinates on p (Y_{cr}), v and t axes are 1, 2 and 3 Å, respectively, and for angles at most 30°. The alignment of **1**–**20** in the common coordinate system v–t–p was performed in the AcrB trimer (PDB: 1OY6 [53]). Parameters ε, ρ and δ_p from AcrB–drug structures (Table 3), connected by obvious geometrical relationships (Fig. 11), were used to determine the center of mass coordinates for **17**–**20**. Besides, due to drug-induced changes in AcrB, δ_p was rescaled with respect to the ratio of values C in the complexed and uncomplexed (C = 6.51 Å) AcrB. The orientation of **17**–**20** in the complexes was preserved in the superposition. Predicted ε, ρ and δ_p for **1**–**16** (Table 4) were used to calculate the center of mass coordinates. Angle ε was the only parameter for the center of mass deviation from the axis v, whilst δ_p had reasonable statistics and rather large variation (Table 4). Besides, ρ was obtained from exact relationships and not regression. For simplicity, it was assumed that the XY and pv were coplanar, i.e. angle A_{zp} = 90°. This required double rotation of **1**–**16** in the v–t–p coordinate system after introducing the molecules into AcrB, first around axis t by 90° counterclockwise, and then around axis v by angle A_{xp} clockwise. The superposition of **1**–**20** inside the central cavity is visible in Fig. 12. It can be said that dipole moment components, polarizability and steric properties related to the principal axes (especially to X) quantitatively determine AcrB–drug geometry (Table 4).

It is visible (Figs. 8 and 9) that a drug may bind to the E wall, E and W ceiling, W wall fused with the SW wall, and the vestibule end. E and W walls are inclined to each other by 60° due to C_3 symmetry (Fig. 6B). There are three binding modes (Fig. 13): interaction with the E binding sites (E binding: DEQ, **1**, **3**, **16**), binding to the W binding sites (W binding: ET, **2**, **5**–**8**, **13**, **15**), and bridging two or more binding sites (bridging: E, W and vestibule binding sites for CPF, RHQ, **4**, **9**–**12**, **14**). Only DEQ is bound to the E ceiling. Obviously, elongated molecules prefer E or vestibule binding site whilst larger molecules with high ramification (RHQ) or flexibility (some cephalosporins) are bridging the binding sites.

Electrostatic potential of **1**–**16** along the axis v (Fig. 12) reveals that hydrophobic, amphiphilic or positively charged regions (R, R_1) in good (**1**, **2**) and most moderate substrates (6/8) are oriented towards the pore, while those in poor substrates (3/4) in opposite direction. **1**–**19** are practically in the same orientation with respect to VP as in Fig. 5. The correlation of AcrB–drug geometry parameters (Table 3: experimental for **17**–**20**, Table 4: predicted for **1**–**16**) with pMICs can be significant (Fig. 14). Groups of substrates may show higher correlations, similarly to pMIC–drug descriptor correlations (Fig. 3). The sample clustering with respect to binding modes and activity classes (previously defined [29] and extended to **17**–**20**) is visible in Fig. 14. Lower pMICs have preference for substrates closer to the protein center (small ρ) and probably orthogonal to the v axis (high A_{yp} and A_{xp}). These correlations, flat drug shape and drug self-association result in weaker drug binding. The correlations (Fig. 14 a–d) show that most bridging drugs (7/8) are poor/moderately good substrates, whilst considerable W binding drugs (5/8) are moderately good substrates. PCA analysis using Pirouette [106] on all autoscaled geometry parameters, shows that the four principal components contain 90.2% of the original information. 3D scores plot (Fig. 14 right) have practically the same sample clustering, with E binding drugs classified as good or moderately good substrates. Thus, the substrate binding to the central cavity receptors could be important step in drug excretion from active (HN891, SH5014) and passive (SH7616) AcrB pumps in *S. typhimurium* strains.

Table 4
Predicted AcrB–substrate geometry for β-lactams **1–16**

Y	Regression equations[a]				Predictions[e]	
	$Y = a(\sigma_a) + b(\sigma_b)X_1 + c(\sigma_c)X_2$	r[b]	p[c]	Δ_{av}[d]	Range	Mean (S.D.)
C	$C = 5.84(30) + 0.000253(73)I_x$	0.926	0.074	0.15	6.2–7.1	6.5 (3)
	$C = 5.47(40) + 0.00251(72)A_{xyz}$	0.927	0.073	0.15		
	$C = 4.79(36) + 0.0155(27)A_{xy}$	0.971	0.029	0.11		
δ_p	$\delta_p = 24.20(216) - 5.48(72)\Delta_{xz}$	0.983	0.017	0.70	6.5–14.0	11.5 (18)
	$\delta_p = 1.36(92) + 0.00517(58)\lvert\beta\rvert$	0.988	0.277	0.57		
	$\delta_p = 42.22(284) - 34.59(287)n_x$	0.993	0.007	0.49		
δ	$\delta = 26.04(697) - 4.90(231)\Delta_{xz}$	0.832	0.168	2.10	10.0–17.1	14.7 (17)
	$\delta = 4.93(239) + 0.00511(151)\lvert\beta\rvert$	0.923	0.175	1.55		
	$\delta = 43.93(1184) - 32.76(1197)n_x$	0.888	0.112	1.76		
ρ[f]	$\rho = [\delta^2 - \delta_p{}^2]^{1/2}$	–	–	–	7.6–9.7	9.1 (5)
R	$R = 33.09(533) - 5.45(177)\Delta_{xz}$	0.909	0.091	1.62	15.4–23.1	20.4 (19)
	$R = 9.85(120) + 0.00553(76)\lvert\beta\rvert$	0.982	0.018	0.74		
	$R = 52.38(780) - 35.80(789)n_x$	0.955	0.045	1.05		
A_{xv}	$A_{xv} = 94.9(45) - 0.92(37)D_x$	0.871	0.129	4.2°	81–106°	94 (7)°
A_{yv}	$A_{yv} = 81.3(60) - 1.7(3)D_z$	0.972	0.028	5.9°	60–120°	83 (14)°
A_{zv}	$A_{zv} = -84.1(518) + 41.8(138)I_{zx}$	0.907	0.246	19.4°	−29 to 69°	13 (29)°
	$A_{zv} = -140.8(547) + 70.4(182)D_{xz}$	0.939	0.124	19.2°		
A_{xp}	$A_{xp} = 434.7(825) - 235.3(619)I_{zy}$	0.937	0.063	10.3°	82–191°	151 (31)°
A_{yp}	$A_{xp} = 415.5(129) - 212.2(866)\Delta_{12}$	0.866	0.134	20.7°	77–215°	146 (36)°
	$A_{xp} = 310.2(1033) - 118.8(582)\Delta_{yz}$	0.822	0.178	24.2°		
	$A_{xp} = -185.5(1311) - 419.3(1878)W_{zy}$	0.845	0.293	21.1°		
A_{zp}	$A_{zp} = 189.6(483) - 73.9(362)I_{zy}$	0.822	0.178	5.6°	82–99°	92 (5)°
	$A_{zp} = 107.6(135) - 0.000229(16)\gamma$	0.995	0.046	0.9°		
	$A_{zp} = -87.4(391) - 194.7(424)\log(W_{Xm})$	0.956	0.155	2.9°		
ε	$\varepsilon = -81.3(310) + 55.2(218)\Delta_{xy} + 13.5(33)(\Delta_{xy})^2$	0.998	0.239	1.5°	−28 to 65°	−1 (24)°
	$\varepsilon = 69.4(80) - 98.2(109)W_{zy} + 199.0(69)(W_{zy})^2$	0.9999	0.073	0.5°		
Π_{xpv}	$\Pi_{xpv} = 254.0(147) - 52.5(48)I_{yx}$	0.992	0.008	6.7°	44–162°	111 (32)°
	$\Pi_{xpv} = 284.4(270) - 49.8(72)I_{zx}$	0.980	0.020	12.3°		
	$\Pi_{xpv} = 737.3(511) - 10.1(8)S_{\%}$	0.994	0.007	6.6°		
Π_{ypv}	$\Pi_{ypv} = 53.7(57) + 12.4(15)I_{zx}$	0.986	0.014	2.3°		100 (12)°
	$\Pi_{ypv} = 253.9(373) - 117.8(280)I_{zy}$	0.948	0.052	4.3°	77–116°	
Π_{zpv}	$\Pi_{zpv} = 415.7(1067) - 26.1(91)\Delta_1 - 0.180(165)(\Delta_1)^2$	0.946	0.472	7.2°	74–182°	131 (33)°
	$\Pi_{zpv} = 416.3(1105) - 26.2(95)W_{YD} - 0.193(172)(W_{YD})^2$	0.942	0.463	7.4°		
Π_{xypv}	$\Pi_{xypv} = 93.4(15) + 1.8(1)D_z$	0.998	0.002	1.5°	54–115°	91 (14)°

[a] Regression equations: Y: dependent variable (an AcrB–drug geometry parameter); a, b, c: regression coefficients; σ_a, σ_b, σ_c: statistical errors of a, b, c, respectively, given in brackets for the last 1–3 digits of the regression coefficients; X_1: molecular descriptor or its simple function (log term); X_2: square term of molecular descriptor. X_1 and X_2 have units as in Table 3.
[b] Correlation coefficient between experimental and calculated values of Y for **17–20**.
[c] Maximum Student's test probability for the regression coefficients.
[d] Average absolute deviation of calculated from experimental values of Y for **17–20**. Units are Å or ° as in Table 3.
[e] Predicted values of Y for **1–16**, as obtained from particular regression equations and then averaged. The range and mean with standard deviation in parentheses are given for these predictions. Units are Å or ° as in Table 3.
[f] Expression based on geometrical relationships as defined in Fig. 11.

3.5. Possible efflux mechanism

AcrAB–TolC (Fig. 1) belongs to the hydrophobe/amphiphile efflux-1 family [1,2]. It is a sophisticated electromechanical device that works in four-phase cycle: the closed state, excited state (opening), open state (drug efflux), and relaxation state (closing). The opening includes primary changes that comprise proton capture by certain acidic residues and disruption of salt bridges (Fig. 15), and secondary changes that include conformational changes within the pump and its components and the AcrB pore opening. Known hydrogen bond-containing conserved residues in MexA [74,75] provoke MexA oligomerization and interaction with OprM during proton efflux. AcrA protomers can oligomerize when protonated and make an impulse to the equatorial domain of TolC which then interacts with the α-domain of TolC [107] facilitating the opening of the TolC pore. The impulse is also transmitted to the TolC bottom which then moves towards the AcrB funnel. PQS analysis [108] of the AcrB trimer (1IWG) shows six interchain salt bridges. The upper triad is placed at the funnel entrance, which when broken, enlarges the funnel so that TolC can dock in it (Fig. 15). The other triad, connecting the vestibule conserved motif to the PDs wall, breaks and the vestibule can enlarge and be more flexible. The protomer bridges (in the TMSs) also contribute to the pore and TMG opening/extending. PQS analysis [108] of TolC (1EK9) displays nine interchain salt bridges: triads in the TolC pore, TolC top (end), and top of the equatorial domain. When TolC cylinder is docking to AcrB funnel, TolC pore

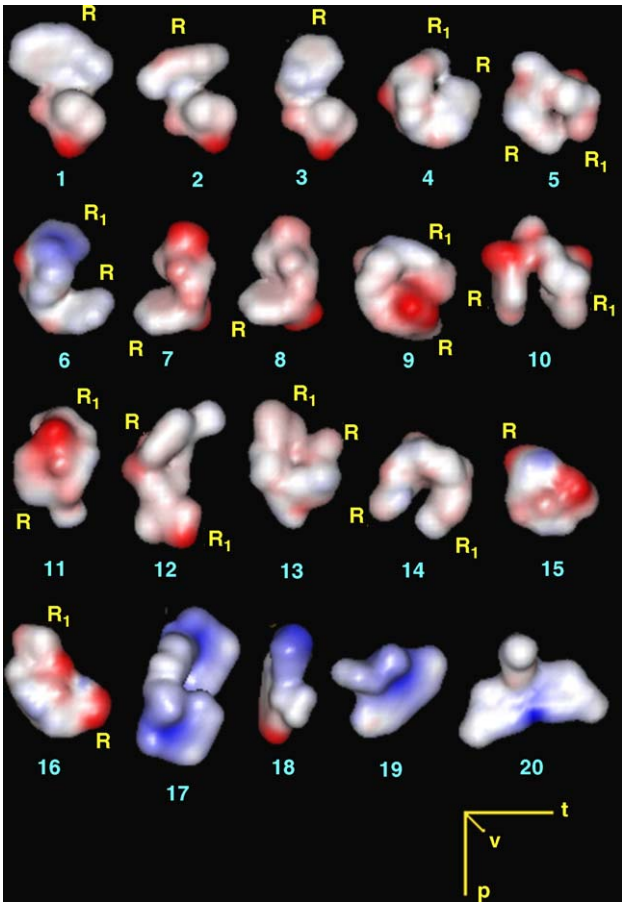

Fig. 12. Electrostatic potential representation of **1**–**20** in the central cavity, viewed along the vestibule axis. Coloring: (red) negative, (blue) positive, (white) zero surface electrostatic potential. Most of drug molecules expose their positive, amphiphilic or hydrophobic heads (substituent R or R_1) towards the predominantly negatively charged ceiling and the pore.

opens and makes the cylinder bottom to widen and tightly connect to the funnel.

Outer membrane of Gram-negative bacteria slows down general drug uptake [33,109], but is susceptible to small drugs (mass < 650 [63] as for **1**–**20**, Fig. 3a). β-Lactams can enter the periplasm or cytoplasm through porin channels or membrane bilayer. Drug efflux pathway consists of a few phases (I–VII, Fig. 15). A periplasmic substrate may interact with the polar headpieces of the inner leaflet (I) and be transported to the vestibule entrance by lateral diffusion (II), or may directly interact with the vestibule (IIc) [50]. A substrate from the cytoplasm might interact with headpieces of the inner leaflet (Ia) and then be turned to the outer leaflet by uncatalyzed lipid flip-flop mechanism (IIb), or transfered by lateral diffusion to the TMG (IIa). Alternatively, it may also interact directly with the TMG (IId). Finally, the TMG may act as a flippase and bring substrates into the neighboring vestibule (IIe) [45]. Single-component efflux pumps in the inner membrane of Gram-negative bacteria excrete cytoplasmic substrates into the periplasm [3]. When working simultaneously with multi-component pumps, they multiplicate the efflux efficiency [64]. This is another option for drug efflux. A drug molecule interacts with the vestibule bypassing it (III), and weakly bounds to the central cavity (IV) [51]. During the efflux, the molecule is attracted by the PRS and transfered by the pore (V) to the funnel (VI) and TolC cylinder (VII). The vestibules and the AcrB pore are considered as drug selection devices [22,52].

Although no specific molecular shape or substructures are needed for drug efflux [24], a number of drug properties accounts drug–phospolipid bilayer interactions [51,110,111]: size, general molecular shape; the presence of charged, polar, hydrogen bonding and aromatic groups; charge distribution; polarity; lipophilicity; permanent dipole moment even being

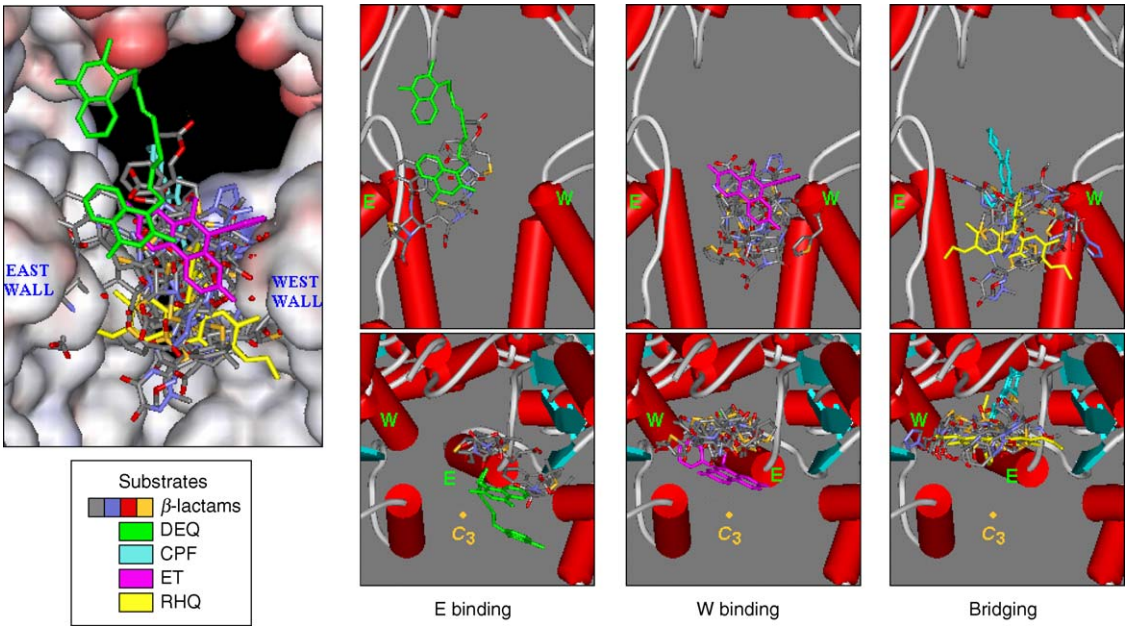

Fig. 13. Superimposed β-lactams and DEQ, CPF, ET and RHQ in the central cavity of the AcrB trimer (left picture: structure 1OY6 represented by electrostatic potential). The position and orientation for **1**–**16** was from predicted AcrB–drug geometry (Table 4) and that of **17**–**20** from experimentally determined structures. The three pairs of the small pictures with schematic representation of the protein illustrate E binding, W binding and bridging binding modes of the substrates in the central cavity.

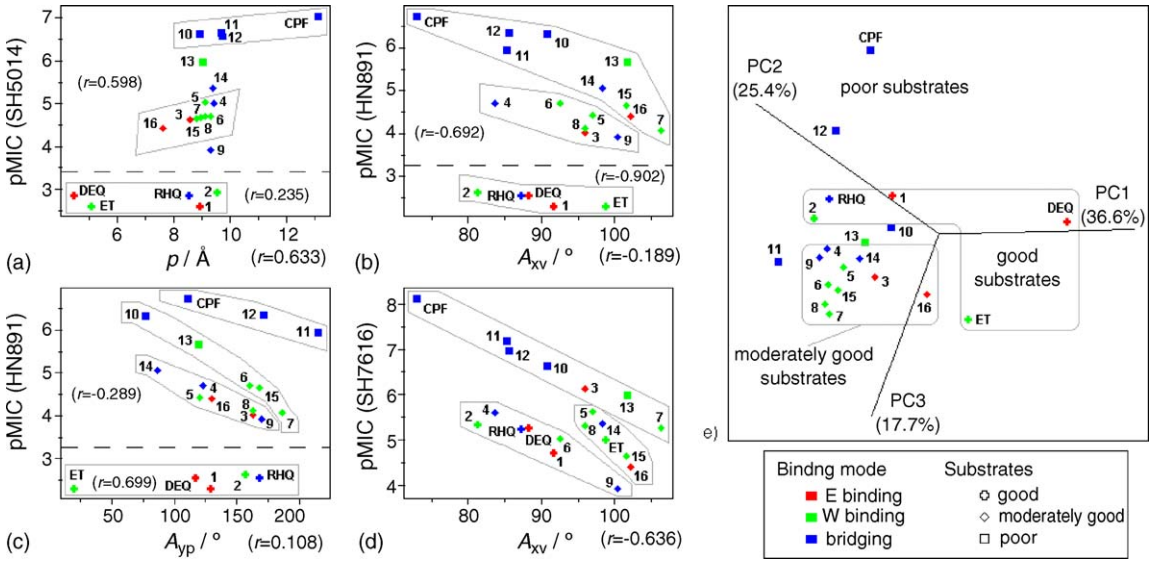

Fig. 14. (a)–(d) Representative correlations between pMICs and AcrB–drug geometry parameters, with correlation coefficients for the complete data set and two subsets (separated by dashed midway line). (e) 3D scores plot from PCA. The tendency of the sample clustering in terms of binding modes and activity classes may be observed by different coloring and legend.

small. Considerable transmembrane potential in bacterial cells [51,112] makes the drug–bilayer interactions to be predominantly electrical. The polar domain of an amphiphilic substrate interacts with the polar headpieces of the leaflets [109]. The polar headpieces, excited by an external potential (i.e. of the drug dipole), extend and place more perpendicular to the membrane plane [112]. β-Lactams, CPF and amphiphilic substrates are positioned into the polar part of the phospolipid bilayer with carboxyl groups, while cationic and polycationic substrates are only absorbed on the bilayer surface [33,51]. The substrate ionization and the local pH may influence the drug–membrane/pump interactions [32]. Dipole moment and its components for **1**–**20** are shown in this and previous work [29] as important for drug efflux. Most moderately good and poor β-lactam substrates have small dipole moment components (Fig. 5). During lateral diffusion (II, IIa in Fig. 15), a substrate molecule maintains its orientation with respect to the inner membrane [51]. Pictorial models of efflux mechanisms [32,33,39,45,49,51] also confirm such substrate orientation in phases I–VII (the substrate lipophilic domain oriented upwards) and flip-flop of substrates coming from the cytoplasm. Linear combinations of dipole moment components for **1**–**16** show the contributions of D_x and D_y and not of D_z to pMICs. For HN891 and SH5014, the increase in correlation between pMICs and the $D_x + D_y$ combination corresponds to a substrate axis in the XY plane, 25–30° away from Y, along which the dipole has the largest influence on drug pMICs. For strain SH7616, the new axis is closer to X (by 25°). Thus, X and Y are

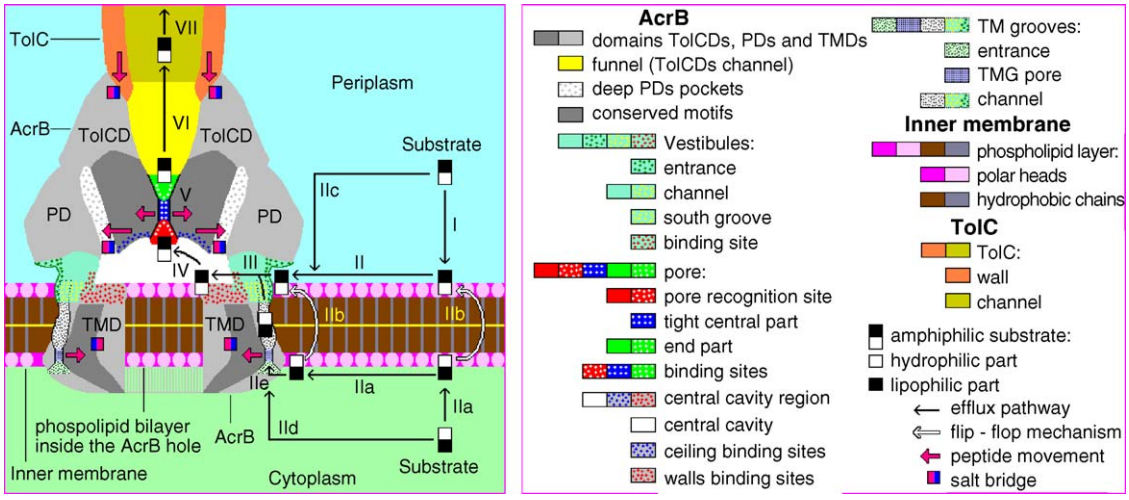

Fig. 15. Schematic representation of the AcrB mediated drug efflux from a Gramm-negative bacteria cell. The efflux component AcrA is excluded because of the clarity. AcrB, TolC and the inner membrane components are colored differently. AcrB is viewed from the direction of the removed protomer, showing thus two symmetrically related protomers. Probable steps (I–VII) are explained in text. Hydrophilic/lipophilic orientation of an amphiphilic drug molecule with respect to the macromolecular systems is also visible. Conserved motifs, salt bridges and principal peptide movements are marked with appropriate symbols.

inclined and not parallel relative to the drug pathway directions (see Section 3.2, Figs. 4 and 5).

The vestibule center lies right above the top of the inner membrane [49] (see Figs. 1, 7b and 8a–c), so the substrates partitioned in the inner leaflet enter directly the closest SG without altering their orientation relative to the phospholipid bilayer [51] (phases II and III, Fig. 15). A qualitative 2D pictorial "docking" of **18–23** and some β-lactams to BRAMLA, was performed (Fig. 16a) taking into account the SC-inner membrane connection, experimental (Fig. 9) and predicted (Figs. 12 and 13) drug–pump geometry, substrate properties (Figs. 3 and 4), and vestibule properties (Fig. 8). All drugs interact with USG (except 21), and glide by their *XY* planes along the surfaces of the SW and E wall. Supposing that the gliding direction is parallel either to *X* or *Y* axis or their midway, there are six distinct substrate orientation groups: large (**1–4**, **6–9**, **11**, **12**), small (**10**, **13**, **15**, **16**), and very small β-lactam group (**5**, **14**); DEQ, CPF; RHQ; the rest (ET, **21–23**). Qualitative analysis of orientation of vectors $D_x + D_y$ shows that their negative ends first enter a vestibule and keep moving along the pathway direction inclined to *X* or *Y* by 30° (see dipole moments, Fig. 5). This agrees with Yu et al. [53] that the hydrophilic head group of a drug would travel through vestibules. Planar fragments in **1**, **18** and **19** glide parallel to SW and E walls.

Österberg and Norinder [23] have noticed the presence of intramolecular hydrogen bonds in substrates of cancer efflux pumps. Similarly, there are bent and U-shaped substrates among **1–16** (Figs. 5 and 12), stabilized by hydrogen bonds and electrostatic interactions. The conformations affect drug position/orientation in vestibules (Fig. 16a and b), the central cavity (Figs. 12 and 13), and PRS (Fig. 16c). Substrates coming from the lipid bilayer or TMG (Fig. 16b) travel through the SG which is narrow at the end and turned to the left. The end is formed by three residues of the SW wall and three of the E wall. This elastic region acts like a trap (one-way door) for substrates, since five residues (their C_α–C_β bonds) are at 105–147° (1IWG) relative to the positive *v* axis, whilst the aromatic plane of the sixth residue (Phe458 from a RND conserved motif, E wall) is inclined by 20°. Fig. 16b shows the centers of masses for **1–20** in the central hole, with corrected positions for some β-lactams along the axis *t*. These positions indicate that the substrates, after leaving the vestibule channel, rotate clockwise/anticlockwise, and simultaneously move in a curvilinear trajectory along positions I–IV or I–III. Substrates may favor binding to the vestibule binding sites a–d (as CPF at I), the W binding sites (II), the E binding sites (IV: DEQ, **1**), and binding to more binding sites (III). Most substrates are located at positions II and III.

Predicted orientation of **1–20** (Figs. 12 and 13) shows hydrophilic end (the positive end of molecular dipoles) sticking towards the acidic residues of the PRS and neighborhood. This agrees with pictorial models of the efflux mechanism [32,33,39,45,49,51]. Among β-lactams complexed by the PRS (Fig. 16c), hydrogen bonds were detected for **8**, **12** and **14**, but not for **1** and **23**, meaning that hydrophilic drugs are bad substrates due to strong binding to the PRS. C_3 symmetry of AcrB and TolC (Figs. 1 and 6) and receptor/recognition sites

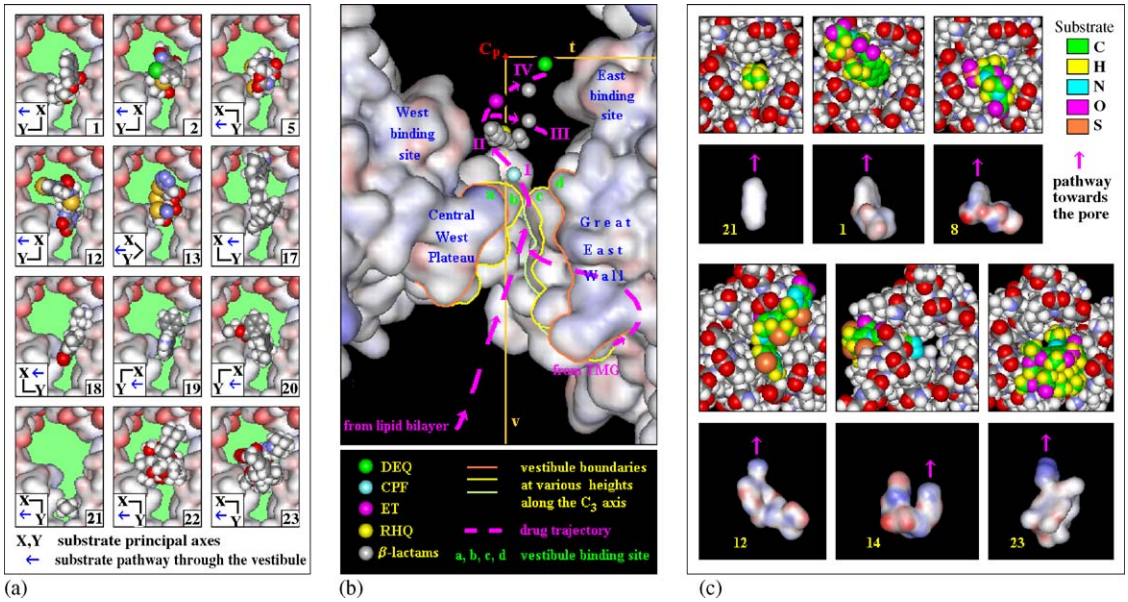

Fig. 16. (a) Representative drug molecules at the vestibule entrance. The orientation of substrates on their way towards the vestibule channel (see the orientation of the *XY* axes) is qualitative. (b) Probable drug pathway through the vestibule and binding to the central cavity/vestibule binding sites. Electrostatic potential of the TMDs (PDB: 1OY6) as viewed downwards the C_3 axis. Both experimental and predicted drugs center of mass positions reveal four possible pathways in the binding area: (I) binding to the vestibule binding sites a–d (E and SW walls at the vestibule end); (II) drug binding to the W binding site in the central hole; (III) drug positioning in the middle of the binding area including interactions with two or three binding sites; (IV) binding to the E binding site. It is supposed that a drug molecule moves along these trajectories untill reaching its best binding position. (c) Selected pore tripeptide–drug complexes. The substrates are colored differently to be distinguished from the pore residues. Free and bound substrates are oriented in such a way that the most hydrophobic fragment (R in β-lactams) goes first into the PRS pocket.

(Figs. 4B–E and 10A, B, G and H) mimics C_6 (Figs. 10D, E and 16c) or even axial symmetry channels. Good substrates should have similar steric and electronic properties, i.e. higher symmetry with respect to their X axes (as good substrates, Figs. 12 and 16c).

Dearden and Thomson [113], in a QSAR study of over 150 phenothiazines with MDR reversal in cancer cells (P-glycoprotein pump), had to analyze compounds of the same class separately and even using different descriptors (similar situation in Fig. 3). It was probably due to different mechanisms of the MDR reversal effects. Among the selected descriptors were I_x and D_y (as in this and previous [29] work), polarization in the XY plane (consistent with this work), electrotopological index for nitrogen atoms (reminding on previous results [29]), polar surface area (polar groups are important as in this work), and the number of aliphatic rings (important for lipophilicity, Section 3.1), among others.

4. Conclusions

AcrAB–TolC is a proton-dependent electromechanical device that opens and closes by a series of conformational changes and rearrangements of at least eighteen inner- and interchain salt bridges. β-Lactams from the periplasm and cytoplasm are partitioned in the layer of polar headpieces of the inner membrane, and by lateral diffusion and transmembrane groove-mediated flip-flop reach vestibules and the central cavity, maintaining orientation relative to the phospholipid bilayer. After being weakly bound in the cavity, they are driven to the pore and then translocated to TolC, and finally excreted from the cell. β-Lactam properties like lipophilicity, molecular shape/conformation, distribution of polar/charged and hydrogen bonding groups define drug-membrane and drug-pump interactions. Good substrates are amphiphilic/lipophilic and elongated molecules with moderate dipole moments. The ends of these dipoles maintain orientation with respect to the efflux system during their excretion. This work will be continued with molecular dynamics and docking studies of pump–substrate interactions and pump structural changes during proton influx.

Acknowledgement

This works was supported by the State of São Paulo Funding Agency (FAPESP).

References

[1] M.H. Saier Jr., A functional-phylogenetic classification system for transmembrane solute transporters, Microbiol. Mol. Biol. Rev. 64 (2000) 354–411.
[2] M.H. Saier Jr., Transport Classication Database. http://www-biology.ucsd.edu/~msaier/transport/ (last access on August 6, 2004).
[3] F. Van Bambeke, Y. Glupczynski, P. Plésiat, J.C. Pechère, P.M. Tulkens, Antibiotic efflux pumps in prokaryotic cells: occurence, impact on resistance and strategies for the future antimicrobial therapy, J. Antimicrob. Chemother. 51 (2003) 1055–1065.
[4] F. Van Bambeke, J.-M. Michot, P.M. Tulkens, Antibiotic efflux pumps in eukaryotic cells: occurence and impact on antibiotic cellular pharmacokinetics, pharmacodynamics and toxicodynamics, J. Antimicrob. Chemother. 51 (2003) 1067–1077.
[5] D.L. Nelson, M.M. Cox, Lehninger Principles of Biochemistry, 3rd. ed., Worth Publishers, New York, 2000.
[6] S. Larriba, L. Bassas, S. Egozcue, J. Giménez, M.D. Ramos, O. Briceño, Adenosine triphosphate-binding cassette superfamily transport gene expression in severe male infertility, Biol. Reprod. 65 (2001) 394–400.
[7] J.W. Klunder, R. Komdeur, W.T.A. Van Der Graaf, E.J.S.M. De Bont, H.J. Hoekstra, E. Van Den Berg, W.M. Molenaar, Expression of multidrug resistance-associated proteins in rhabdomyosarcomas before and after chemotherapy: the relationship between lung resistance-related protein (LRP) and differentiaion, Hum. Pathol. 34 (2003) 150–155.
[8] I.T. Paulsen, M.H. Brown, R.A. Skurray, Proton-dependent multidrug efflux systems, Microbiol. Rev. 60 (1996) 575–608.
[9] M. Putman, H.W. Van Veen, W.N. Konings, Molecular properties of bacterial multidrug transporters, Microbiol. Mol. Biol. Rev. 64 (2000) 672–693.
[10] G.J.R. Zaman, M.J. Flens, M.R. Van Leusden, M. De Haas, H.S. Mülder, J. Lankelma, H.M. Pineado, R.J. Sheper, F. Baas, H.J. Broxterman, P. Borst, The human multidrug resistance-associated protein MRP is a plasma drug–efflux pump, Proc. Natl. Acad. Sci. U.S.A. 91 (1994) 8822–8826.
[11] D. De Wet, D.B. McIntosh, G. Conseil, H. Baubichon-Cortay, T. Krell, J.-M. Jault, J.-B. Daskiewicz, D. Barron, A. Di Pietro, Sequence requirements of the ATP-binding site within the C-terminal nucleotide-binding domain of mouse P-glycoprotein: structure-activity relationships for flavonoid binding, Biochemistry 40 (2001) 10382–10391.
[12] M.H. Kollef, Selective digestive decontamination should not be routinely employed, Chest 123 (2003) 464S–468S.
[13] D.J. Austin, K.G. Kristinsson, R.M. Anderson, The relationship between the volume of antimicrobial consumption in human communities and the frequency of resistance, Proc. Natl. Acad. Sci. U.S.A. 96 (1999) 1152–1156.
[14] K.M. Shea, Antibiotic resistance: what is the impact of agricultural uses of antibiotics on children's health? Pediatrics 112 (2003) 253–258.
[15] S.B. Levy, Antimicrobial resistance: bacterial on the defense, Br. Med. J. 317 (1998) 612–613.
[16] S.B. Levy, Multidrug resistance—a sign of the times, N. Engl. J. Med. 338 (1998) 1376–1378.
[17] J.M.C. Saller, M.J.C. Salles, Antimicrobianos, EDUFPA, Belém, PA, Brazil, 2000.
[18] R.J. Williams, D.L. Heymann, Containment of antibiotic resistance, Science 279 (1998) 1153–1154.
[19] P. Houvinen, O. Cars, Control of antimicrobial resistance: time for action, Br. Med. J. 317 (1998) 613.
[20] F.J. Esteva, V. Valero, L. Pusztai, L. Boehnke-Michaud, A.U. Buzdar, G.N. Hortobagyi, Chemotherapy of metastasic breast cancer: what to expect in 2001 and beyond, Oncologist 16 (2001) 133–146.
[21] P.N. Markham, E. Westhaus, K. Klyachko, M.E. Johnson, A.A. Neyfakh, Multiple novel inhibitors of the NorA multidrug transporter of *Staphylococcus aureus*, Antimicrob. Agents Chemother. 43 (1999) 2404–2408.
[22] M. Malléa, A. Mahamoud, J. Chevalier, S. Alibert-Franco, P. Brouant, Alkylamonquinolines inhibit the bacterial antibiotic efflux pump in multidrug-resistant clinical isolates, Biochem. J. 376 (2003) 801–805.
[23] T. Österberg, U. Norinder, Theoretical calculation and prediction of P-glycoprotein-interacting drugs using MolSurf parametrization and PLS statistics, Eur. J. Pharm. Sci. 10 (2000) 295–303.
[24] J.C. Dearden, QSAR of Pgp efflux, in: Proceedings of the 14th European Symposium on Quantitative Structure-Activity Relationships: Workshop 1—Drug Transporters. Can they be Modelled?, Bournemouth, UK, September 8–13, (2002, http://www.mgsm.org/euroqsar_workshop.htm (last access on August 9, 2004).
[25] V.K. Gombar, J.W. Polli, J.E. Humphreys, S.A. Wring, C.S. Serabjit-Singh, Predicting P-glycoprotein substrates by a quantitative structure–activity relationship model, J. Pharm. Sci. 93 (2004) 957–968.
[26] S. Ekins, R.B. Kim, B.F. Leake, A.H. Dantzig, E.G. Schuetz, L.-B. Lan, K. Yasuda, R.L. Shepard, M.A. Winters, J.D. Schuetz, J.H. Wikel, S.A. Wrighton, Three-dimensional quantitative structure–activity relation-

ships of inhibitors of P-glycoprotein, Mol. Pharmacol. 61 (2002) 964–973.
[27] B. Gopalakrishnan, A. Khandelwal, S.A. Rajjak, N. Selvakumar, J. Das, S. Trehan, J. Igbal, M.S. Kumar, Three-dimensional studies of tricyclic oxazolidinones as antibacterial agents, Bioorg. Med. Chem. 11 (2003) 2569–2574.
[28] D.T. Stanton, P.J. Madhar, L.J. Wilson, T.W. Morris, P.M. Hershberger, C.N. Parker, Development of a quantitative structure–activity relationship model for inhibition of gram-positive bacterial cell growth by biarylamides, J. Chem. Inf. Comput. Sci. 44 (2004) 221–229.
[29] M.M.C. Ferreira, R. Kiralj, QSAR study of β-lactam antibiotic efflux by the bacterial multidrug resistance pump AcrB, J. Chemometr. 18 (2004) 242–252.
[30] R.A. Powers, B.K. Stoichet, Structure-based approach for binding site identification on AmpC β-lactamase, J. Med. Chem. 45 (2002) 3222–3234.
[31] E. Gordon, N. Mouz, E. Dueé, O. Dideberg, The crystal structure of the penicillin-binding protein 2× from *Streptococcus pneumoniae* and its acyl-enzyme form: implication in drug resistance, J. Mol. Biol. 299 (2000) 477–485.
[32] F. van Bambeke, F. Balzi, P.M. Tulkens, Antibiotics efflux pumps, Biochem. Pharmacol. 60 (2002) 457–470.
[33] H. Nikaido, Multidrug efflux pumps of gram-negative bacteria, J. Bacteriol. 178 (1996) 5853–5859.
[34] M. Sulavik, C. Houseweart, C. Cramer, N. Jiwani, N. Murgolo, J. Greene, B. Di Domenico, K.J. Shaw, G.H. Millear, R. Hare, G. Shimer, G. Antibiotic susceptibility of *Escherichia coli* strains lacking multidrug efflux pump genes, Antimicrob. Agents Chemother. 45 (2001) 1126–1136.
[35] E. Giraud, A. Cloekaert, D. Kerboeuf, E. Chaslus-Dancla, Evidence for active efflux as the primary mechanism of resistance to ciprofloxacin in *Salmonella enterica* serovar typhimurium, Antimicrob. Agents Chemother. 44 (2000) 1223–1228.
[36] H. Okusu, D. Ma, H. Nikaido, AcrAB efflux pump plays a major role in the antibiotic resistance phenotype of *Escherichia coli* multiple-antibiotic-resistance (mar) mutants, J. Bacteriol. 178 (1996) 306–308.
[37] H.I. Zgurskaya, H. Nikaido, Bypassing the periplasm: reconstitution of the AcrAB multidrug efflux pump of *Escherichia coli*, Proc. Natl. Acad. Sci. U.S.A. 96 (1999) 7190–7195.
[38] R.B. Helling, B.K. Janes, H. Kimball, T. Tran, M. Budesmann, P. Check, D. Phelan, C. Miller, Toxic waste disposal in *Escherichia coli*, J. Bacteriol. 184 (2002) 3699–3703.
[39] H. Nikaido, M. Basina, V. Nguyen, E.Y. Rosenberg, Multidrug efflux pump AcrB of *Salmonella typhimurium* exctretes only those β-lactam antibiotics containing lipophilic side chains, J. Bacteriol. 180 (1998) 4686–4692.
[40] L. Sanchez, W. Pan, M. Vinas, H. Nikaido, The acrAB homolog of *Hamemophilus influenzae* codes for a functional multidrug efflux pump, J. Bacteriol. 179 (1997) 6855–6857.
[41] R. Aono, N. Tsukagoshi, M. Yamamoto, Involvement of outer membrane protein TolC, a possible member of the mar–sox regulon, in maintenance and improvement of organic solvent tolerance of *Escherichia coli* K12, J. Bacteriol. 180 (1998) 938–944.
[42] D.G. Thanassi, L.W. Cheng, H. Nikaido, Active efflux of bile salts by *Escherichia coli*, J. Bacteriol. 179 (1997) 2512–2518.
[43] D.G. White, J.D. Goldman, B. Demple, S.B. Levy, Role of the acrAB locus in organic solvent tolerance mediated by expression of marA, soxS, or robA in *Escherichia coli*, J. Bacteriol. 179 (1997) 6122–6126.
[44] N. Tamura, S. Konishi, A. Yamaguchi, Mechanism of drug/H+ antiport: complete cysteine-scanning mutagenesis and the protein engineering approach, Curr. Opin. Chem. Biol. 7 (2003) 570–579.
[45] S. Murakamai, A. Yamaguchi, Multidrug-exporting secondary transporters, Curr. Opin. Struct. Biol. 13 (2003) 443–452.
[46] S. Murakami, R. Nakashima, E. Yamashita, A. Yamaguchi, Crystal structure of bacterial multidrug efflux transporter AcrB, Nature 419 (2002) 587–593.
[47] K.M. Pos, K. Diederichs, Purification, crystallization and preliminary diffraction studies of AcrB, an inner-membrane multi-drug efflux protein, Acta Cryst. D58 (2002) 1865–1867.
[48] H. Zgurskaya, H. Nikaido, Bypassing the periplasm: Reconstitution of the AcrAB multidrug efflux pump of *Escherichi coli*, Proc. Natl. Acad. Sci. U.S.A. 96 (1999) 7190–7195.
[49] K.M. Pos, A. Schiefner, M.A. Seeger, K. Diederichs, Crystallographic analysis of AcrB, FRBS Lett. 564 (2004) 333–339.
[50] C.A. Elkins, H. Nikaido, 3D structure of AcrB: the archetypal multidrug efflux tranporter of *Escherichia coli* likely captures substrates from periplasm, Drug Resist. Updates 6 (2003) 9–13.
[51] E.W. Yu, J.R. Aires, H. Nikaido, AcrB multidrug efflux pump of *Escherichia coli*: composite substrate-binding cavity of exceptional flexibility generates its extremely wide substrate specificity, J. Bacteriol. 185 (2003) 5657–5664.
[52] S. Murakami, N. Tamura, A. Saito, T. Hirata, A. Yamaguchi, Extra-membrane central pore of multidrug exporter AcrB in *Escherichi coli* plays an important role in drug transport, J. Biol. Chem. 279 (2004) 3743–3748.
[53] E.W. Yu, G. McDermott, H.I. Zgurskaya, H. Nikaido, D.E. Koshland Jr., Structural basis of multiple drug-binding capacity of the AcrB multidrug efflux pump, Science 300 (2003) 976–980.
[54] V. Koronakis, A. Sharff, E. Koronakis, B. Luisi, C. Hughes, Crystal structure of the bacterial membrane protein TolC central to multidrug efflux and protein export, Nature 405 (2000) 914–919.
[55] A. Sharff, C. Fanutti, J. Shi, C. Calladine, B. Luisi, The role of the TolC family in protein transport and multidrug efflux, Eur. J. Biochem. 268 (2001) 5011–5026.
[56] C. Andersen, E. Koronakis, E. Bokma, J. Eswaran, D. Humphreys, C. Hughes, V. Koronakis, Transition to the open state of the ToIC periplasmic tunnel entrance, Proc. Natl. Acad. Sci. U.S.A. 99 (2002) 11103–11108.
[57] T. Thanabalu, E. Koronakis, C. Hughes, V. Koronakis, Substrates-induced assembly of a contiguous channel from protein export from *E. coli*: reversible bridging for an inner-membrane translocase to an outer membrane exit pore, EMBO J. 17 (1998) 6487–6496.
[58] A.J. Avila-Sakar, S. Misaghi, E.M. Wilson-Kubalek, K.H. Downing, H.I. Zgurskaya, H. Nikaido, E. Nogales, Lipid-layer crystallization and preliminary three-dimensional structural analysis of AcrA, the periplasmic component of a bacterial multidrug efflux pump, J. Struct. Biol. 136 (2001) 81–88.
[59] H.I. Zgurskaya, H. Nikaido, Cross-linked complex between oligomeric periplasmic lipoprotein AcrA and the inner-membrane-associated multidrug efflux pump AcrB from *Eschrichia coli*, J. Bacteriol. 182 (2000) 4264–4267.
[60] H. Ip, K. Stratton, H. Zgurskaya, J. Liu, pH-induced conformational changes of AcrA, the membrane fusion protein of *Escherichia coli* multidrug efflux system, J. Biol. Chem. 278 (2003) 50474–50482.
[61] T. Dinh, I.T. Paulsen, M.H. Saier Jr., A family of extracytoplasmic proteins that allow transport of large molecules across the outer membranes of gram-negative bacteria, J. Bacteriol. 176 (1994) 3825–3831.
[62] J.A. Fralick, Evidence that TolC is required for functioning of the Mar/AcrAB efflux pump in *Escherichia coli*, J. Bacteriol. 178 (1996) 5803–5805.
[63] H. Nikaido, Microdermatology: cell surface in the interaction of microbes with the external world, J. Bacteriol. 181 (1999) 4–8.
[64] A. Lee, W. Mao, M.S. Warren, A. Mistry, K. Hoshino, R. Okumura, H. Ishida, O. Lomovskaya, Interplay between efflux pumps may provide either additive or multiplicative effects on drug resistance, J. Bacteriol. 182 (2000) 3142–3150.
[65] C.A. Elkins, H. Nikaido, Substrate specificity of the RND-type multidrug efflux pumps AcrB and AcrD of *Escherichia coli* is determined predominantly by two large periplasmic loops, J. Bacteriol. 184 (2002) 6490–6498.
[66] WebLab ViewerPro, version 4.0, Accelrys, Inc., Burlington, MA, 2000.
[67] M. Bartuluchi, G. Sevlever, A.L. Taratuto, Multidrug resistance proteins in *Tuberou sclerosis* and refractory epilepsy, Pediatric Neurol. 30 (2004) 102–106.

[68] H.M. Berman, J. Westbrook, Z. Feng, G. Gilliland, T.N. Bhat, H. Weissig, I.N. Shindyalov, P.E. Bourne, The Protein Data Bank, Nucl. Acids Res. 28 (2000) 235–242.
[69] The Protein Data Bank, The Research Collaboratory for Structural Bioinformatics, http://www.rcsb.org/pdb/ (last access on August 9, 2004).
[70] E. Fujihira, N. Tamura, A. Yamaguchi, Membrane topology of a multidrug efflux transporter, AcrB, in *Escherichia coli*, J. Bacteriol. 131 (2002) 145–151.
[71] E.B. Tikhonova, Q. Wang, H.I. Zgurskaya, Chimeric analysis of the multicomponent multidrug efflux transporters from gram-negative bacteria, J. Bacteriol. 184 (2002) 6499–6507.
[72] L. Guan, M. Ehrmann, H. Yoneyama, T. Nakae, Membrane topology of the xenobiotic-exporting subunit, MexB, of the MexA. B-OprM extrusion pump in *Pseudomonas aeruginosa*, J. Biol. Chem. 274 (1999) 10517–10522.
[73] K.K.Y. Wong, F.S.L. Brinkman, R.S. Benz, R.E.W. Hancock, Evaluation of a structural model of *Pseudomonas aeruginosa* outer membrane protein OprM, and efflux component involved in intrinsic antibotic resistance, J. Bacteriol. 183 (2001) 367–374.
[74] H. Akama, T. Matsuura, S. Kashiwagi, H. Yoneyama, S.-I. Narita, T. Tsukihara, A. Nakagawa, T. Nakae, Crystal structure of the membrane fusion protein, MexA, of the multidrug transporter in *Pseudomonas aeruginosa*, J. Biol. Chem. 279 (2004) 25939–25942.
[75] M.K. Higgins, E. Bokma, E. Koronakis, C. Hughes, V. Koronakis, Structure of the periplasmic component of a bacterial drug efflux pump, Proc. Natl. Acad. Sci. U.S.A. 101 (2004) 9994–9999.
[76] R. Wise, Maximizing efficacy and reducing the emergence of resistance, J. Antimicrob. Chemother. 51 (Suppl. S1) (2003) 37–42.
[77] D. Ma, D.N. Cook, M. Alberti, N.G. Pon, H. Nikaido, J.E. Hearst, Genes acrA and acrB encode a stress-induced efflux system of *Escherichi coli*, Mol. Microbiol. 16 (1995) 45–55.
[78] A.A. Neyfakh, Mystery of multidrug transporters: the answer can be simple, Mol. Microbiol. 44 (2002) 1123–1130.
[79] I.T. Paulsen, Multidrug efflux pumps and resistance: regulation and evolution, Curr. Opin. Microbiol. 6 (2003) 446–451.
[80] A. Dobashi, 3D Pharmaceutical Structure Database, Department of Structural Organic Chemistry, Tokyo University of Pharmacy and Life Science, Tokyo. http://www.ps.toyaku.ac.jp/dobashi/3dpsd/index.htm (last access on August 7, 2004).
[81] PC Spartan Pro, Version 1.0.5, Wavefunction Inc., Irvine, CA, 2001.
[82] Lobanov VS MOPAC 6.0 for Microsoft Windows, University of Florida, 1996.
[83] A.L. Spek, PLATON—A Multipurpose Crystallographic Tool 31000, Utrecht University, The Netherlands, 2000.
[84] Matlab, Version 6.1.0.450, Release 12.1, MathWorks, Inc., Natick, MA, 2001.
[85] R. Kiralj, M.M.C. Ferreira, A priori molecular descriptors in QSAR: a case of HIV-1 protease inhibitors. II. Molecular graphics and modeling, J. Mol. Graph. Mod. 21 (2003) 499–515.
[86] T.A. Halgren, Merck molecular force field. 1. Basis, form, scope, parameterization, and performance of MMFF94, J. Comp. Chem. 17 (1996) 490–519.
[87] H. Martens, T. Naes, Multivariate Calibration, 2nd ed., Wiley, New York, NY, 1989.
[88] K.R. Beebe, R. Pell, M.B. Seasholtz, Chemometrics: A Practical Guide, Wiley, New York, NY, 1998.
[89] Ferreira MMC, A.M. Antunes, M.S. Melo, P.L.O. Volpe, Chemometrics I: multivariate calibration, a tutorial, Quím. Nova 22 (1999) 724–731.
[90] P. Geladi, B.R. Kowalski, Partial least squares regression—a tutorial, Anal. Chim. Acta 185 (1986) 1–17.
[91] M.M.C. Ferreira, Multivariate QSAR, J. Braz. Chem. Soc. 13 (2002) 742–753.
[92] M. Dutta, N.N. Dutta, K.G. Bhattacharyya, Adsorptive interaction of certain β-lactam antibiotics in aqueous solution: interpretation by frontier-orbital theory, J. Chem. Eng. Jpn. 33 (2000) 303–307.
[93] S. Leon, C. Alemán, M. García-Alvarez, S. Muñoz-Guerra, Theoretical study of the conformational and electrostatic properties of C4-monosubstituted 2-azetidinones, Struct. Chem. 8 (1997) 39–47.
[94] C. Andersen, Chennel-tunnels: outer membrane components of type I secretion systems and multidrug efflux pumps of Gram-negative bacteria, Rv. Physiol. Biochem. Pharmacol. 147 (2003) 122–165.
[95] M. Masi, J.-M. Pagès, E. Pradel, Overexpression and purification of the three components of the *Enterobacter aerogenes* AcrA–AcrB–TolC multidrug efflux pump, J. Chromatogr. B 876 (2003) 197–205.
[96] C.A. Elkins, H. Nikaido, Chimeric analysis of AcrA function reveals the importance of Its C-terminal domain in its interaction with the AcrB multidrug efflux pump, J. Bacteriol. 185 (2003) 5349–5356.
[97] R. Srikumar, T. Kon, N. Gotoh, K. Poole, Expression of *Pseudomonas aeruginosa* multidrug efflux pumps MexA-MexB-OprM and MexC-MexD-OprJ in a multidrug-sensitive *Escherichia coli* strain, Antimicrob. Agents Chemother. 42 (1998) 65–71.
[98] C. Andersen, E. Koronakis, C. Hughes, V. Koronakis, An aspartate ring at the TolC tunnel entrance determines ion selectivity and presents a target for blocking by large cations, Mol. Microbiol. 44 (2002) 1131–1139.
[99] E. Fujihira, N. Tamura, A. Yamaguchi, Membrane topology of a multidrug efflux transporter AcrB, in *Escherichia coli*, J. Biochem. 131 (2002) 145–151.
[100] O.P. Hamill, B. Martinac, Molecular basis of mechanotransduction in living cells, Physiol. Rev. 81 (2001) 685–740.
[101] W. Rawicz, K.C. Olbrich, T. McIntosh, D. Needham, E. Evans, Effect of chain length and unsaturation on elasticity of lipid bilayers, Biophys. J. 79 (2000) 328–339.
[102] D. Uhríkova, N. Kučerka, A. Islamov, V. Gordeliy, P. Balgavý, Small-angle neutron scattering study of the lipid bilayer in unilamellar dioeloylphosphatidylcholine liposomes prepared by the cholate dilution method: *n*-decane effect, Biochim. Biophys. Acta 1611 (2003) 31–34.
[103] L.P. McIntosh, E. Brun, L.E. Kay, Stereospecific assignment of the NH_2 resonances from the primary amides of asparagine and glutamine side chains in isotropically labeled proteins, J. Biomol. NMR 9 (1997) 306–312.
[104] Chem3D Ultra 8.0, CambridgeSoft.Com, Cambridge, MA, 2000.
[105] N.L. Allinger, Conformational Analysis.130. MM2—hydrocarbon force-field utilizing v1 and V2 torsional terms, J. Am. Chem. Soc. 99 (1977) 8127–8134.
[106] Pirouette 3.02, Infometrix, Woodinville, WA, 2001.
[107] H. Yamanaka, H. Izawa, K. Okamoto, Carboxy-terminal region involved in activity of *Escherichia coli* TolC, J. Bacteriol. 183 (2001) 6961–6964.
[108] PQS Protein Quaternary Structure Query Form at the EBI—The Macromolecular Structure Database, EMBL-EBI (European Bioinformatics Institute). http://pqs.ebi.ac.uk/ (last access on August 18, 2004).
[109] B. Lakaye, A. Dubus, B. Joris, J.-M. Frère, Method for estimation of low outer membrane permeability to β-lactam antibiotics, Antimicrob. Agents Chemother. 46 (2002) 2901–2907.
[110] A.S. Kulkarni, A.J. Hopfinger, Membrane-interaction QSAR analysis: application to the estimation of eye irritation by organic compounds, Pharm. Res. 16 (1999) 1245–1253.
[111] X. Hong, A.J. Hopfinger, Molecular modeling of *Mycobacterium tuberculosis* cell wall permeability, Biomacromolecules 5 (2004) 1066–1077.
[112] A. Le Saux, J.-M. Ruysschaert, E. Goormaghtigh, Membrane molecule reorientation in an electric field recorded by attenuated total reflection Fourier-transform infrared spectroscopy, Biophys. J. 80 (2001) 324–330.
[113] J.C. Dearden, S.A. Thomson, QSAR study of reversal of multidrug resistance by phenothiazines, http://www.rpsgb.org.uk/events (last access on 25 August 2004), in: Proceedings of the 140th British Pharmaceutical Conference, Harrogate, UK, September 15–17, (2003.